



HAL
open science

The topological gradient method for semi-linear problems and application to edge detection and noise removal.

Audric Drogoul, Gilles Aubert

► **To cite this version:**

Audric Drogoul, Gilles Aubert. The topological gradient method for semi-linear problems and application to edge detection and noise removal.. 2015. hal-01018200v2

HAL Id: hal-01018200

<https://hal.science/hal-01018200v2>

Preprint submitted on 7 Jan 2015 (v2), last revised 30 Oct 2015 (v3)

HAL is a multi-disciplinary open access archive for the deposit and dissemination of scientific research documents, whether they are published or not. The documents may come from teaching and research institutions in France or abroad, or from public or private research centers.

L'archive ouverte pluridisciplinaire **HAL**, est destinée au dépôt et à la diffusion de documents scientifiques de niveau recherche, publiés ou non, émanant des établissements d'enseignement et de recherche français ou étrangers, des laboratoires publics ou privés.

The topological gradient method for semi-linear problems and application to edge detection and noise removal.

Audric Drogoul and Gilles Aubert

7 janvier 2015

AUDRIC DROGOUL

Univ. Nice Sophia Antipolis, CNRS, LJAD, UMR 7351, 06100 Nice, France
drogoula@unice.fr

GILLES AUBERT

Univ. Nice Sophia Antipolis, CNRS, LJAD, UMR 7351, 06100 Nice, France
gaubert@unice.fr

Résumé

The goal of this paper is to apply the topological gradient method for segmenting/restoring images degraded by various noises and blurs. First applied by Hintermuller [Control and Cybernetics, 34 (2005), pp. 305-324] and Belaid et al [C. R. Acad. Sci. Paris, 342 (2006), pp.313-318] to restore images degraded by a Gaussian noise, we propose here to extend the method to blurred images contaminated either by an additive Gaussian noise, or a multiplicative noise of gamma law and to blurred Poissonian images. We compute, both for perforated and cracked domains, the topological gradient for each noise model. Then we present a segmentation/restoration algorithm based on this notion and we apply it to the three degradation models previously described. We compare our method with the Ambrosio-Tortorelli approximation of the Mumford-Shah functional and with those given by a classical TV restoration process. Many experimental results showing the efficiency, the robustness and the rapidity of the approach are presented.

1 Introduction

An important problem in image analysis is the reconstruction of an original image u from an observed image f . In general this includes restoration and segmentation processes. The transformation between f and u originates from two phenomena. The first phenomenon is related to the acquisition process (blur created by a wrong lens adjustment or by a movement, Poissonian photons emission rates ...) and the second is due to the signal transmission. A lot of methods to reconstruct such degraded images exist : stochastic methods [22, 13], wavelets decomposition [31, 18], morphological methods [36]. Here we are interested with variational approaches [7]. In this context, the most famous model is the Mumford-Shah functional [33] (1989) but other works based on variational methods do exist ([7]). Among more recent papers, we can cite [8] (2008) for restoration of images contaminated by speckle noise, [16] (2014) for blind restoration of Poissonian images, and [35] (2013) for an overview of image restoration degraded by different type of noise.

In this paper we tackle the segmentation problem by using the topological gradient method. First introduced for cracks detection by Sokolowski and Zochowski [37], Masmoudi [32] and applied in

optimal design and mechanics ([3], [2], [4]), this notion consists in the study of the variations of a cost function $j(\Omega) = J_\Omega(u_\Omega)$ with respect to a topological variation, where $J_\Omega(u)$ is of the form $J_\Omega(u) = \int_\Omega F(u, \nabla u, \nabla^2 u, \dots)$ and u_Ω is a solution of a PDE defined on the image domain Ω . In order to compute the topological gradient, we remove to Ω a small object ω_ε of size $\varepsilon \rightarrow 0$ centered at $x_0 \in \Omega$ (generally a ball or a curve) and we set $\Omega_\varepsilon = \Omega \setminus \overline{\omega_\varepsilon}$. Two typical examples are : for small $\varepsilon > 0$ (a) $\Omega_\varepsilon = \Omega \setminus \{x_0 + \varepsilon B\}$ and (b) $\Omega_\varepsilon = \Omega \setminus \{x_0 + \varepsilon \sigma(n)\}$, where $B = B(O, 1)$ is the unit ball of \mathbb{R}^2 and $\sigma(n)$ is a straight segment with normal n (a crack). We compute the limit : $\mathcal{S}(x_0) = \lim_{\varepsilon \rightarrow 0} \frac{j(\Omega_\varepsilon) - j(\Omega)}{\varepsilon^d}$ where d is the dimension of the ambient space. $\mathcal{S}(x_0)$ is called the topological gradient at x_0 . It measures the energy contained by a perturbation centered at x_0 and so the structures that we want to detect correspond to the points x_0 where $\mathcal{S}(x_0)$ is the largest. The type of structure to be detected depends on the choice of the cost function $J_\Omega(u)$. Recently this notion has been used in image processing and to the best of our knowledge the first works in this direction are those by [25], [30], [14]. Then other imaging problems such as inpainting, classification, demosaicing, super resolution, have been addressed using a topological gradient approach ([9, 15], [12, 11], [10], [28], [29]). In [14], only Gaussian additive noise is considered and no blur has been introduced. Blur has been introduced in [29]. In fact, in [29] more general degradations have been taken into account. The authors consider model of the form $f = Lu + b$ where f is the observed image, L a linear operator and b a Gaussian additive noise. They compute in the case of a crack the topological gradient and illustrate their approach for various imaging problems (segmentation/restoration, super resolution, demosaicing). Note also that topological gradient methods have been also applied for fine structures detection (e.g. points and filaments) [6], [5], [20]. In this case the cost function is based on second order derivatives. Restoration/segmentation in imaging are in general ill-posed inverse problems and one way to overcome this difficulty is to regularize them. A classical framework to do that is to use a Bayesian formulation which leads to the minimization of an energy consisting in two terms. The first one is a data fidelity term which takes into account both the statistic of the noise and the blur and the second one is an adequate regularizing term. For example if we suppose that the acquisition model is of the form $f = u + b$ where b is Gaussian noise then an anti-log-likelihood estimator amounts to choose as a data fidelity term the L^2 norm $\|u - f\|_{L^2(\Omega)}$. If the noise follows another statistic, of course this term changes. The regularizing term is often based on an L^p norm of the gradient. Our main contribution is to generalize the results given in [29] to blurred images contaminated by speckle noise and Poissonian statistic and to give the different expression of the topological gradient associated to the cost function $J_\Omega(u) = \int_\Omega |\nabla u|^2$. More precisely we will consider variational problems of the following form

Speckle and Gaussian noise model :

$$\min_{u \in H^1(\Omega)} \frac{\gamma}{2} J_\Omega(u) + \int_\Omega \psi(x, Ku) \quad (1)$$

Poissonian model :

$$\min_{u \in H^1(\Omega)} \frac{\gamma}{2} J_\Omega(u) + \sum_{j \in I_{ind}(\Omega)} \psi_j \left(\int_{R_j} Ku \right) \quad (2)$$

where $I_{ind}(\Omega)$ is the indices set of pixels, $\gamma > 0$ is a parameter, R_j is a regular domain modeling pixel j such that Ω is the disjoint union of $(R_i)_{i \in I_{ind}(\Omega)}$, $K : L^2(\Omega) \rightarrow L^2(\Omega)$ is a convolution operator (generally positive and such that $K\mathbb{1} \neq 0$) representing the blur. The functions $\psi(x, u)$ and $\psi_j(v)$ will be specified in section 5 and section 6. Note that problems (1) and (2) are semi-linear and one of our contribution is to show they are well-posed and verify some maximum principles. Speckle noise is a multiplicative noise of gamma law, which is present in SAR images, laser images, microscope images

[27, 24, 38]. A Poisson statistic occurs in confocal microscopy [19], emission tomography [39] and single-photon emission computed tomography [23].

In section 2, we recall the classical rationale justifying the modelization of the data fidelity term in a Bayesian approach. In section 3 we set the variational problem taking into account the blurring. Then in section 4, we give the topological gradient for a blurred and Gaussian noisy image. In section 5 we show that problem (1) is well-posed and compute the associated topological gradient both for perforated and cracked domains (in fact, we study a more general class of problem (1)). In section 6 we treat the Poissonian model (2) whose energy is not standard. We summarize in Table 1 (section 7) all the expressions of the topological gradient according to the type of noise and to the infinitesimal perturbation. In section 8 we show how to apply the notion of topological gradient to restore degraded images. Finally in section 9, we present, for all the models, a detailed numerical analysis for computing the topological gradient and we display various experimental results illustrating each of them.

We conclude this section by giving some notations and assumptions : we suppose to simplify that $x_0 = 0$ and we denote by $\|u\|_{m,\Omega}$ the $H^m(\Omega)$ -norm of the Sobolev space $H^m(\Omega) = \{u, D^\alpha u \in L^2(\Omega), |\alpha| \leq m\}$ and by $\|u\|_{H^1(\Omega)/\mathbb{R}}$ the norm on the quotient space $H^1(\Omega)/\mathbb{R}$. We set $J_\Omega(u) = \int_\Omega |\nabla u|^2$ and $J_{\Omega_\varepsilon}(u) = J_\varepsilon(u)$.

Only the proof for a perforated domain is performed since for a cracked domain the explicit dependency on the data is killed by the fact that the crack has a null Lebesgue measure. Hence we just give the topological gradient expression for a cracked domain (b) and develop the full proof for a perforated domain (a).

2 A Bayesian approach

In this section we recall the classical Bayesian approach allowing to deduce the suitable variational model for restoring noisy images. We denote N the number of pixels in the support of the image Ω . The discrete domain is denoted Ω^N . We set u^N (respectively f^N) the discrete version of the image u to recover (respectively of the observed image f). For each pixels $p_x \in \Omega^N$, $f^N(p_x)$ and $u^N(p_x)$ can be viewed as a realization of the random variables $U^N(p_x)$ and $F^N(p_x)$ where U^N and F^N stand for the random vector formed by these variables at each pixel. We suppose that they are identically distributed and independent. The reasoning is as follows : we express the a priori density probability $g_{U^N|F^N}$ and then we search for u^N as the value maximizing this density probability (a Maximum A Priori estimator). A discrete model associated to a discrete energy is deduced and then passing to the limit when $N \rightarrow \infty$ we get the continuous variational model. Let $g_{U^N|F^N}$ be the a posteriori density probability that we want to maximize with respect to u^N . Thanks to the Bayes rule, $g_{U^N|F^N}$ expresses as :

$$g_{U^N|F^N} = \begin{cases} \frac{g_{(F^N, U^N)}}{g_{F^N}} = \frac{g_{F^N|U^N} g_{U^N}}{g_{F^N}}, & \text{if } g_{F^N} > 0 \\ 0, & \text{otherwise} \end{cases}$$

$g_{F^N|U^N}$ depends on the noise model and g_{U^N} is an a priori density probability. Writing that u^N is a minimum of $-\log(g_{U^N|F^N})$ we get

$$u^N = \underset{u}{\operatorname{argmin}} E^N(u)$$

where

$$E^N(u) = -\log(g_{F^N|U^N}(u, f)) - \log(g_{U^N}(u)) \quad (3)$$

The a priori density g_{U^N} has to be determined, it will play the role of a regularizing term. In analogy to statistical mechanics, a priori densities are frequently Gibbs functions [22] of the form :

$$g_{U^N}(u) = C \times e^{-\frac{\gamma}{2}J^N(u)}, \quad \gamma > 0$$

where $J^N(u)$ is a discrete version of a non negative energy functional $J_\Omega(u)$ and C is a constant. The choice of the density probability $g_{F^N|U^N}$ depends on the statistic of the model to be considered. Below we review respectively the Gaussian model, the speckle model and finally the Poisson model.

Gaussian model

A classical modeling of image formations is : $F^N = U^N + G^N$ where U^N is the discrete version of the image to recover and G^N a Gaussian noise of mean 0 and of standard deviation σ . The density of the Gaussian noise is $g_{G^N}(x) = \frac{1}{\sqrt{2\pi}\sigma} e^{-\frac{x^2}{2\sigma^2}}$. To simplify we still denote by F^N , S^N and U^N the random variables $F^N(p_x)$, $S^N(p_x)$ and $U^N(p_x)$. Let us express the conditional probability density $g_{F^N|U^N}$. From the definition of the conditional probability we have :

$$P(F^N \in \mathcal{A} | U^N = u) = \int_{\mathbb{R}} g_{F^N|U^N}(f|u) \mathbb{1}_{f \in \mathcal{A}} df \quad (4)$$

The conditional probability density $g_{F^N|U^N}(f|u)$ is a function of the variable f and depending on a parameter u . From the model $F^N = U^N + G^N$, the independency of U^N and G^N and a change of variable we get

$$\begin{aligned} P(F^N \in \mathcal{A} | U^N = u) &= P(U^N + G^N \in \mathcal{A} | U^N = u) \\ &= P(G^N \in \mathcal{A} - U^N | U^N = u) \\ &= P(G^N \in \mathcal{A} - u) \\ &= \int_{\mathbb{R}} g_{G^N}(x) \mathbb{1}_{x \in \mathcal{A} - u} dx \\ &= \int_{\mathbb{R}} g_{G^N}(f - u) \mathbb{1}_{f \in \mathcal{A}} df \end{aligned}$$

Hence by identification with (4) we deduce that $g_{F^N|U^N}(f|u) = g_{G^N}(f - u)$. Thanks to the independency hypothesis, the density of $F^N|U^N$ is the product with respect to each pixel p_x of the densities $F^N(p_x)|U^N(p_x)$. So the energy given in (3) rewrites in this case (up to a multiplicative constant) as

$$E^N(u) = \sum_{p_x \in \Omega^N} \frac{1}{\sigma^2} (f^N - u)^2 + \gamma J^N(u) + C$$

with C a constant non depending on u . The constant σ^2 can be neglected in the model because it can be scaled with the regularization parameter γ . By passing to the limit when $N \rightarrow +\infty$, we get the following continuous energy

$$E(u) = \int_{\Omega} (f - u)^2 + \gamma J_\Omega(u)$$

Speckle model

For SAR images, the classical modeling is (see [38]) : $F^N = S^N U^N$ where U^N is the reflectance of the scene (which is to be recovered) and S^N the speckle noise. Let us explicit the law of S^N . SAR

images are constructed from $L \in \mathbb{N}$ observations F_k^N for $1 \leq k \leq L$ and for each observations we have $F_k^N = G_k^N U^N$. Generally G_k^N is a random variable which follows a negative exponential law with mean 1 and with density $g_G(x) = e^{-x} \mathbb{1}_{\{x \geq 0\}}$. Then, the observed image F^N is construct from this L observations as : $F^N = \frac{1}{L} \sum_{k=1}^L F_k^N = \left(\frac{1}{L} \sum_{k=1}^L G_k^N \right) U^N$. We set $S^N = \frac{1}{L} \sum_{k=1}^L G_k^N$; S^N follows a gamma law with density $g_{S^N}(x) = \frac{L^L}{\Gamma(L)} x^{L-1} e^{-Lx} \mathbb{1}_{\{x \geq 0\}}$ with $\Gamma(L) = (L-1)!$ (the mean of S^N is 1 and its variance $\frac{1}{L}$). Now we can express the density $g_{F^N|U^N}$. To simplify we still denote by F^N , S^N and U^N the random variables $F^N(p_x)$, $S^N(p_x)$ and $U^N(p_x)$. We start from the definition of the conditional probability :

$$P(F^N \in \mathcal{A} | U^N = u) = \int_{\mathbb{R}} g_{F^N|U^N}(f|u) \mathbb{1}_{\{f \in \mathcal{A}\}} df \quad (5)$$

where $g_{F^N|U^N}(f|u)$ is a function of the variable f and depending on a parameter u . Then, from the model $F^N = S^N U^N$ and the independency of U^N and S^N we have :

$$\begin{aligned} P(F^N \in \mathcal{A} | U^N = u) &= P(S^N U^N \in \mathcal{A} | U^N = u) \\ &= P(S^N \in \frac{\mathcal{A}}{U^N} | U^N = u) = P(S^N \in \frac{\mathcal{A}}{u}) \end{aligned}$$

Thanks to the definition of P and by a change of variable we get :

$$P\left(S^N \in \frac{\mathcal{A}}{u}\right) = \int_{\mathbb{R}} g_{S^N}(s) \mathbb{1}_{\{s \in \frac{\mathcal{A}}{u}\}} = \int_{\mathbb{R}} \frac{1}{u} g_{S^N}\left(\frac{f}{u}\right) \mathbb{1}_{\{f \in \mathcal{A}\}} df$$

Then by identification with (5), we deduce that

$$g_{F^N|U^N}(f|u) = \frac{1}{u} g_{S^N}\left(\frac{f}{u}\right) \quad (6)$$

From the independency $F^N(p_x)$ and $U^N(p_x)$, the density of $F^N|U^N$ is the product with respect to pixels p_x of the densities $F^N(p_x)|U^N(p_x)$. By taking the $-\log$ function we deduce that (3) rewrites in this case as

$$E^N(u) = L \sum_{p_x \in \Omega^N} \left(\frac{f^N}{u} + \log(u) \right) + \frac{\gamma}{2} J^N(u) + C$$

for $u \in \mathbb{R}^N$ and $u > 0$, where C denotes a constant independent of u . The factor L can be neglected since it can be scaled with the constant γ . Passing to the limit as $N \rightarrow \infty$, we deduce the following continuous energy

$$E(u) = \int_{\Omega} \left(\frac{f}{u} + \log(u) \right) dx + \frac{\gamma}{2} J_{\Omega}(u) \quad (7)$$

Speckle with Log of the image (Speckle-Log model)

One drawback of (7) is that it is nonconvex. By setting, $v = \text{Log}(u)$ and $g = \text{Log}(f)$, we deduce from (7) the expression of the data fidelity term in function of v and we introduce the following energy function :

$$E(v) = \int_{\Omega} v + e^{-(v-g)} + \frac{\gamma}{2} J_{\Omega}(v) \quad (8)$$

which is now a convex function of v . The recovered image is then $u = e^v$.

Poissonian model

This model is classical in astronomical and confocal microscopy images [19]. Poissonian observations originates from the stochastic nature of photons emission. We denote R_j , for $j \in I_{ind}(\Omega)$, the domain of \mathbb{R}^2 modeling pixel j and such that Ω is the disjoint union of all the $(R_j)_{j \in I_{ind}(\Omega)}$. We assume that f is a step function constant on each R_j and we still denote $f^N = f$ the observed image seen as the realization of the random vector F .

More precisely for $j \in I_{ind}(\Omega)$, f_j is a realization of a Poisson statistic of mean and variance equal to $\lambda_j^N = \int_{R_j} u^N(x) dx$ where $x \mapsto u^N(x)$ is a discrete version of $u^N \in \mathbb{R}^N$ (may be a step function or a bi-linear interpolation). Thanks to the independence of F_j and U_j^N , the conditional probability $P(F = f | U^N = u)$ is given by :

$$P(F = f | U^N = u) = \prod_{j \in I_{ind}(\Omega)} \frac{\lambda_j^N f_j e^{-\lambda_j^N}}{f_j!}$$

and by applying the $-\log$ function, we have :

$$-\log(P(F = f | U^N = u)) = \sum_{j \in I_{ind}(\Omega)} \lambda_j^N - f_j \log(\lambda_j^N) + C$$

where C is constant independent of u . We deduce that (3) rewrites in this case as

$$E^N(u) = \sum_{j \in I_{ind}(\Omega)} (\lambda_j^N - f_j \log(\lambda_j^N)) + \frac{\gamma}{2} J^N(u)$$

The dependence of E^N with respect to u comes from the definition of λ^N . Passing to the limit we get the continuous energy :

$$E(u) = \sum_{j \in I_{ind}(\Omega)} \left(\int_{R_j} u(x) dx - f_j \log \left(\int_{R_j} u(x) dx \right) \right) + \frac{\gamma}{2} J_{\Omega}(u) \quad (9)$$

3 Blurring modeling

In most imaging applications the optical material, the motion of the camera or of the target introduce a blur on the observed image (see [34]). Generally spatially invariant blur is modeled as a positive convolution operator $u \mapsto Ku$ with $K\mathbb{1} \neq 0$. We denote by K^N the $N \times N$ matrix associated to the discrete version of K on Ω^N . From section 2 we deduce the following models adapted to each kind of noise and taking into account the blur :

1. Gaussian model : the observed image writes as $F^N = K^N U^N + G^N$ and by the same reasoning of section 2 we get the following energy :

$$E(u) = \int_{\Omega} (f - Ku)^2 + \gamma J_{\Omega}(u) \quad (10)$$

2. Speckle model : the observed image writes as $F^N = S^N K^N U^N$ and the energy is

$$E(u) = \int_{\Omega} \log(Ku) + \frac{f}{Ku} + \frac{\gamma}{2} J_{\Omega}(u) \quad (11)$$

3. Speckle model with the Log of the image (Speckle-Log model). We recall that the model writes as $G^N = V^N + T^N$ with $V^N = \log(K^N U^N)$. The deblurring cannot be handled simultaneously with the denoising process. After the denoising step we must solve the problem $V^N = \log(K^N U^N)$ where the unknown U^N can be found by a least square formula :

$$U^N = ((K^N)^T K^N)^{-1} (K^N)^T e^{V^N}$$

but we know that this problem is ill-posed, particularly when K contains small eigenvalues. For this reason the blurring problem is not handled for speckle noise by our method. In this case, if we only want to correctly restore a blurred and speckled image it is preferable to use (11).

4. Poissonian model : the observed image at pixel p_x is a realization of a Poisson statistic of mean $\int_{R_{p_x}} K u^N(x) dx$, so the energy is

$$E(u) = \sum_{p_x \in \text{Ind}(\Omega)} \left(\int_{R_{p_x}} K u(x) dx - f(p_x) \log \left(\int_{R_{p_x}} K u(x) dx \right) \right) + \frac{\gamma}{2} J_\Omega(u) \quad (12)$$

In the sequel we give the topological gradient for the Gaussian and Poisson models with blur and for the Speckle-Log model without blur.

4 Gaussian noise with blurring

We consider problem (1) with the energy (10) :

$$\min_{u \in H^1(\Omega)} \gamma J_\Omega(u) + \int_\Omega \psi(x, Ku) \quad (13)$$

with $\psi(x, v) = (f(x) - v)^2$. We do not give the computation of the topological gradient here because of the similarity with the case without blurring (see [4], [29]). We just give the topological gradient expression and some experimental results. Note that this expression only needs the resolution of two problems : the direct and the adjoint problems (we will see in the next section why an adjoint problem is necessary). By following the notations used in [4], the direct and the adjoint problems u_0 and v_0 are given in this case by :

$$(\mathcal{P}_0) \begin{cases} -\gamma \Delta u_0 + K^* K u_0 = K^* f, & \text{in } \Omega \\ \partial_n u_0 = 0, & \text{on } \partial\Omega \end{cases} \quad (14)$$

and

$$(\mathcal{Q}_0) \begin{cases} -\gamma \Delta v_0 + K^* K v_0 = K^* (2K u_0 - f), & \text{in } \Omega \\ \partial_n v_0 = 0, & \text{on } \partial\Omega. \end{cases} \quad (15)$$

We can show (see [7] chapter 3) that problems (\mathcal{P}_0) and (\mathcal{Q}_0) are well-posed in $H^1(\Omega)$ as soon as $K\mathbb{1} \neq 0$ and $\gamma > 0$. The topological gradients at $x_0 \in \Omega$ for a perforated domain (a) $\Omega_\varepsilon = \Omega \setminus \overline{\{x_0 + \varepsilon B\}}$ and for a cracked domain (b) $\Omega_\varepsilon = \Omega \setminus \overline{\{x_0 + \varepsilon \sigma\}}$, denoted respectively by $I_{Lap}^b(x_0)$ and $I_{Lap}^c(x_0)$ can be easily deduced from the case without blur and are given in the following Theorem.

Theorem 4.1. *The topological gradients associated to problems (14) and (15) and to the cost function $J_\varepsilon(u) = \int_{\Omega_\varepsilon} |\nabla u|^2$, for a perforated and a cracked domain are respectively :*

$$I_{Lap}^b(x_0) = -2\pi \nabla u_0(x_0) \cdot \nabla v_0(x_0) + \frac{\pi}{\gamma} (f(x_0) - K u_0(x_0)) (K v_0(x_0) - K u_0(x_0)) \quad (16a)$$

$$I_{Lap}^c(x_0) = \min_{\|\vec{n}\|=1} \mathcal{J}(x_0, \vec{n}) \quad (16b)$$

$$\text{with } \mathcal{J}(x_0, \vec{n}) = -\pi \nabla u_0(x_0) \cdot \vec{n} \nabla v_0(x_0) \cdot \vec{n}$$

with u_0 and v_0 given by (14) and (15) and $\gamma > 0$.

5 Speckle multiplicative noise

We consider the variational problem (1) with the energy given in (8). More precisely we study the minimization problem :

$$\min_{u \in H^1(\Omega)} \frac{\gamma}{2} J_\Omega(u) + \int_\Omega \psi(x, u) \quad (17)$$

where $\psi(x, u) = u + e^{-(u-g(x))}$ and $g = \log(f)$ is the logarithm of the observed image. We assume that there is no blur i.e. K is the identity operator. To shorten notations we write sometimes $\psi(u)$ instead of $\psi(x, u)$.

Remark 1. In [8] the authors propose a speckle denoising model using the total variation model with the data fidelity term associated to (7).

This section is organized as follows. First, we show that (1) admits a unique solution for a more general class of functions ψ (verifying Hypotheses 1) and we prove that the solution verifies some min/max principles. Then we apply the general result to show that problem (17) admits a unique solution with $\psi(x, u) = u + e^{-(u-g(x))}$. Next, we compute the topological gradient for a general function ψ verifying Hypotheses 1. We still denote $J_\Omega(u) = \int_\Omega |\nabla u|^2$ and $E_\Omega(u) = \frac{\gamma}{2} J_\Omega(u) + \int_\Omega \psi(x, u)$.

5.1 Well-posedness of problem (1)

In this subsection we first establish the well-posedness of (1) for a general class of functions $\psi(x, u)$ and then we check that the function $\psi(x, u)$ associated to the speckle-Log model (17) matches these hypotheses. To simplify we suppose that $\gamma = 1$ and sometimes we write $\psi(u)$ for $\psi(x, u)$.

Hypotheses 1. Let $\psi : \Omega \times I \rightarrow \mathbb{R}$ such that

- (i) $u \mapsto \psi(x, u) \in C^3(I) \forall x \in \bar{\Omega}$
- (ii) $x \mapsto D_u \psi(x, u) \in C^0(\Omega) \forall u \in I$
- (iii) $u \mapsto \psi(x, u)$ is strictly convex on I , uniformly with respect to $x \in \Omega$.
- (iv) ψ is bounded from below on $\Omega \times I$
- (v) $\exists a, b \in I$ such that for all x , $D_u \psi(x, a) \leq 0$ and $D_u \psi(x, b) \geq 0$ with $[a, b] \subset I$.

Lemma 5.1. Let $\psi(x, u)$ a function verifying Hypotheses 1, then (1) admits a unique solution $u_\Omega \in H^1(\Omega)$ such that $a \leq u_\Omega \leq b$.

Démonstration. **Existence :** Let (u_n) a minimizing sequence. There exists a constant C_1 such that $E_\Omega(u_n) \leq C_1$. As $\psi(x, u)$ is bounded from below on $\Omega \times I$ there exists a constant C_2 such that $\int_\Omega \psi(x, u_n) \leq C_2$. Therefore :

$$\int_\Omega |\nabla u_n|^2 \leq \max(C_1, C_1 - C_2)$$

Let $v_n = \max(u_n, a)$, and $\Omega_n^- = \Omega \cap \{u_n \leq a\}$, we have $v_n \geq a$ and

$$E_\Omega(v_n) - E_\Omega(u_n) = - \int_{\Omega_n^-} |\nabla u_n|^2 + \int_{\Omega_n^-} \psi(a) - \psi(u_n)$$

By convexity :

$$\psi(u_n) - \psi(a) \geq D_u \psi(a)(u_n - a) \text{ and } \int_{\Omega_n^-} (\psi(a) - \psi(u_n)) \leq \int_{\Omega_n^-} D_u \psi(a)(a - u_n) \leq 0.$$

We easily deduce that $E_\Omega(v_n) \leq E_\Omega(u_n)$. Thus v_n is still a minimizing sequence and $v_n \geq a$. Similarly by setting $w_n = \min(v_n, b)$, we get $w_n \leq b$ and w_n is a minimizing sequence. Therefore we can suppose that any minimizing sequence u_n verifies $a \leq u_n \leq b$. It is easily seen that u_n is bounded in $H^1(\Omega)$. Thus, up to a subsequence there exists $u \in H^1(\Omega)$ such that $u_n \xrightarrow{L^2(\Omega)} u$ and $u_n \xrightarrow{H^1(\Omega)} u$ (where $\xrightarrow{H^1(\Omega)}$ stands for the weak topology). By using the lower semi-continuity of $J_\Omega(u)$ and Fatou's Lemma we get that u is a solution of (1). Moreover we have $a \leq u \leq b$ a.e. on Ω .

Uniqueness : From the existence, we can work on the set $H(\Omega) = \{v \in H^1(\Omega), a \leq v \leq b\}$. Since $\psi(u)$ is strictly convex on $[a, b] \subset I$ and $J_\Omega(u)$ is strictly convex on $H^1(\Omega)$, we deduce that $E_\Omega(u)$ is strictly convex on $H(\Omega)$ which is a convex set and that E_Ω has a unique minimum in $H^1(\Omega)$.

We apply below Lemma 5.1 to the speckle-Log model. □

Proposition 1. *Let f a function such that $\forall x, 0 < \alpha \leq f(x) \leq \beta$ where α and β are two constants, then problem (17) with $\phi(u) = |\nabla u|^2$ and $\psi(x, u) = u + e^{-(u-g(x))}$ where $g = \log(f)$ has a unique solution $u \in H^1(\Omega)$ and $\forall x, \log(\alpha) \leq u \leq \log(\beta)$.*

Démonstration. A standard computation leads to $D_u \psi(u) = 1 - e^{-(u-g)}$ and $D_u^2 \psi(u) = e^{-(u-g)} > 0$. Hence $\psi(u)$ is strictly convex on $] -\infty, \eta] \forall \eta \in \mathbb{R}$. By using that $0 < \alpha \leq f \leq \beta$ we get

$$1 - e^{-(u-\log(\beta))} \leq D_u \psi(u) \leq 1 - e^{-(u-\log(\alpha))}$$

Let $a = \log(\alpha)$ and $b = \log(\beta)$, the following inequalities hold

$$D_u \psi(b) \geq 0 \text{ and } D_u \psi(a) \leq 0$$

From Lemma 5.1, there exists a unique function $u \in H^1(\Omega)$ solution of (17). Moreover we have $a \leq u \leq b$. □

In the next subsection we detail the computation of the topological gradient for a perforated domain and we just give the result for a cracked domain.

5.2 Computation of the topological gradient for a perforated domain

Let $u_\varepsilon = u_{\Omega_\varepsilon}$ be the solution of problem (1) replacing Ω by $\Omega_\varepsilon = \Omega \setminus \overline{\{x_0 + \varepsilon B\}}$ and let $J_\varepsilon(u) = J_{\Omega_\varepsilon}(u)$. In order to establish the topological expansion for a more general class of problems, we assume that $\psi(x, u)$ verifies Hypotheses 1. By writing that $DE_{\Omega_\varepsilon}(u_\varepsilon) \cdot v = 0$ for all $v \in H^1(\Omega_\varepsilon)$, we obtain the following variational formulation : find $u_\varepsilon \in H^1(\Omega_\varepsilon)$ such that

$$\int_{\Omega_\varepsilon} \gamma \nabla u_\varepsilon \cdot \nabla v + D_u \psi(x, u_\varepsilon) v = 0 \quad \forall v \in H^1(\Omega_\varepsilon) \quad (18)$$

Then by an integration by parts, u_ε necessarily verifies the Euler equations :

$$(\mathcal{P}_\varepsilon) \left\{ \begin{array}{l} -\gamma \Delta u_\varepsilon + D_u \psi(x, u_\varepsilon) = 0 \text{ on } \Omega_\varepsilon \\ \partial_n u_\varepsilon = 0 \text{ on } \partial \Omega_\varepsilon \end{array} \right. \quad (19)$$

If F_ε stands the following functional

$$F_\varepsilon(u, v) = \int_{\Omega_\varepsilon} \gamma \nabla u \cdot \nabla v + D_u \psi(x, u) v \quad \forall u, v \in H^1(\Omega_\varepsilon) \quad (20)$$

Then (18) rewrites as : find $u_\varepsilon \in H^1(\Omega_\varepsilon)$ such that $F_\varepsilon(u_\varepsilon, v) = 0 \quad \forall v \in H^1(\Omega_\varepsilon)$.

We denote by u_0 the solution of (18) for $\varepsilon = 0$ and we state the main result of this section. To simplify notations we perform the proof with $\gamma = 1$ (but we state the Theorem with $\gamma > 0$).

Theorem 5.2. *The topological gradient I_{Lap}^b associated to problem (19) with $\psi(x, u)$ verifying Hypotheses 1 and with the cost function $J_\varepsilon(u) = \int_{\Omega_\varepsilon} |\nabla u|^2$ for a perforated domain is*

$$I_{Lap}^b(x_0) = -2\pi \nabla u_0(x_0) \cdot \nabla v_0(x_0) + \frac{\pi}{\gamma} D_u \psi(x_0, u_0) (u_0(x_0) - v_0(x_0)) \quad (21)$$

with u_0 and v_0 given by (19) and (26) for $\varepsilon = 0$ and with $\gamma > 0$.

Remark 2. The topological sensitivity for some non linear PDEs using as main operator the Laplace operator with Dirichlet boundary conditions (on the boundary of the small perturbation) has been studied by Amstutz [2].

Démonstration. The proof is very technical and can be skipped by readers not interested by details. The topological gradient is given by the leading term in the difference $J_\varepsilon(u_\varepsilon) - J_0(u_0)$. Let us introduce the functional $\tilde{J}_\varepsilon(u) = - \int_{\Omega_\varepsilon} D_u \psi(x, u) u$; by using (18) with $v = u_\varepsilon$, it is straightforward that :

$$\begin{aligned} J_\varepsilon(u_\varepsilon) - J_0(u_0) &= \tilde{J}_\varepsilon(u_\varepsilon) - \tilde{J}_0(u_0) \\ &= - \int_{\Omega_\varepsilon} (D_u \psi(u_\varepsilon) u_\varepsilon - D_u \psi(u_0) u_0) + \int_{B_\varepsilon} D_u \psi(u_0) u_0 \\ &= - \int_{\Omega_\varepsilon} D_u \psi(u_0) (u_\varepsilon - u_0) + (D_u \psi(u_\varepsilon) - D_u \psi(u_0)) u_0 \\ &\quad + \int_{\Omega_\varepsilon} (D_u \psi(u_\varepsilon) - D_u \psi(u_0)) (u_\varepsilon - u_0) \\ &= L_\varepsilon(u_\varepsilon - u_0) + \mathcal{J}_\varepsilon + \mathcal{E}_1 \end{aligned} \quad (22)$$

where

$$\begin{aligned} L_\varepsilon(u) &= - \int_{\Omega_\varepsilon} (D_u \psi(u_0) u + D_u^2 \psi(u_0) u_0 u) \\ \mathcal{J}_\varepsilon &= \int_{B_\varepsilon} D_u \psi(u_0) u_0 \\ \mathcal{E}_1 &= - \int_{\Omega_\varepsilon} \left(\frac{1}{2} D_u^3 \psi(u_{\eta_\varepsilon}) u_0 + D_u^2 \psi(u_{\delta_\varepsilon}) \right) (u_\varepsilon - u_0)^2 \end{aligned} \quad (23)$$

and where $u_{\delta_\varepsilon} = \theta_1 u_0 + (1 - \theta_1) u_\varepsilon$, $u_{\eta_\varepsilon} = \theta_2 u_0 + (1 - \theta_2) u_\varepsilon$ with $\theta_i : \Omega \mapsto \mathbb{R}$, $0 \leq \theta_i \leq 1$ for $1 \leq i \leq 2$. To compute the term $L_\varepsilon(u_\varepsilon - u_0)$ in (22) it is classical [3, 37] to introduce an adjoint problem. Due to the non linearity of the direct problem, we first make a second order Taylor expansion of $F_\varepsilon(u, v)$ with respect to u at point u_0 :

$$\begin{aligned} F_\varepsilon(u_\varepsilon, v) &= F_\varepsilon(u_0, v) + D_u F_\varepsilon(u_0, v) \cdot (u_\varepsilon - u_0, v) + \frac{1}{2} D_u^2 F_\varepsilon(u_{\delta_\varepsilon}, v) \cdot (u_\varepsilon - u_0, u_\varepsilon - u_0) \\ &= F_\varepsilon(u_0, v) + b_\varepsilon(u_\varepsilon - u_0, v) + c_\varepsilon(u_\varepsilon - u_0, u_\varepsilon - u_0, v) \end{aligned} \quad (24)$$

with

$$\begin{aligned} b_\varepsilon(u, v) &= DF_\varepsilon(u_0, v) \cdot u = \int_{\Omega_\varepsilon} \nabla u \cdot \nabla v + \int_{\Omega_\varepsilon} D_u^2 \psi(u_0) uv \quad , \\ c_\varepsilon(u, t, v) &= \frac{1}{2} D_u^2 F_\varepsilon(u_{\delta_\varepsilon}, v) \cdot (u, t) = \int_{\Omega_\varepsilon} \frac{1}{2} D_u^3 \psi(u_{\eta_\varepsilon}) utv \end{aligned}$$

Then the adjoint solution $v_\varepsilon \in H^1(\Omega_\varepsilon)$ is defined as :

$$b_\varepsilon(u, v_\varepsilon) = -L_\varepsilon(u) \quad \forall u \in H^1(\Omega_\varepsilon) \quad (25)$$

The Euler equations associated with (25) are :

$$(\mathcal{Q}_\varepsilon) \begin{cases} -\gamma \Delta v_\varepsilon + D_u^2 \psi(u_0) v_\varepsilon = D_u \psi(u_0) + D_u^2 \psi(u_0) u_0 \text{ on } \Omega_\varepsilon \\ \partial_n v_\varepsilon = 0 \text{ on } \partial \Omega_\varepsilon \end{cases} \quad (26)$$

Remark 3. (i) In the proof, we take $\gamma = 1$.

(ii) The adjoint problem $(\mathcal{Q}_\varepsilon)$ is linear and we can notice that the strict convexity of $u \mapsto \psi(x, u)$ is necessary to $(\mathcal{Q}_\varepsilon)$ be coercive. Since $u \mapsto \psi(x, u)$ is $C^2(I)$ and thanks to Lemma 5.1 there exist two constants $A, B \in \mathbb{R}$ such that

$$A < D_u \psi(u_0) + D_u^2 \psi(u_0) u_0 < B$$

Hence (26) is well-posed and thanks to Lemma 5.1, we have the following inequality

$$\frac{A}{\sup_\Omega D_u^2 \psi(u_0)} \leq v_\varepsilon \leq \frac{B}{\inf_\Omega D_u^2 \psi(u_0)}$$

We deduce from (22) and (24) that :

$$\begin{aligned} J_\varepsilon(u_\varepsilon) - J_0(u_0) &= -b_\varepsilon(u_\varepsilon - u_0, v_\varepsilon) + \mathcal{J}_\varepsilon + \mathcal{E}_1 \\ &= F_\varepsilon(u_0, v) - F_\varepsilon(u_\varepsilon, v_\varepsilon) + c_\varepsilon(u_\varepsilon - u_0, u_\varepsilon - u_0, v_\varepsilon) + \mathcal{J}_\varepsilon + \mathcal{E}_1 \\ &= F_\varepsilon(u_0, v_\varepsilon) + \mathcal{E}_2 + \mathcal{J}_\varepsilon + \mathcal{E}_1 \end{aligned} \quad (27)$$

with

$$\mathcal{E}_2 = c_\varepsilon(u_\varepsilon - u_0, u_\varepsilon - u_0, v_\varepsilon) \quad (28)$$

By using an integration by parts, the term $F_\varepsilon(u_0, v_\varepsilon)$ expresses as :

$$\begin{aligned} F_\varepsilon(u_0, v_\varepsilon) &= \int_{\Omega_\varepsilon} \nabla u_0 \cdot \nabla v_\varepsilon + D_u \psi(u_0) v_\varepsilon \\ &= - \int_{\partial B_\varepsilon} \partial_n u_0 v_\varepsilon + \int_{\Omega_\varepsilon} (-\Delta u_0 + D_u \psi(u_0)) v_\varepsilon \\ &= - \int_{\partial B_\varepsilon} \partial_n u_0 w_\varepsilon - \int_{\partial B_\varepsilon} \partial_n u_0 v_0 \end{aligned}$$

with $w_\varepsilon = v_\varepsilon - v_0$. Now for $\varphi \in H^{1/2}(\partial B_\varepsilon)$ we introduce the following extension on B_ε :

$$\begin{cases} \Delta l_\varepsilon^\varphi = 0, \text{ on } B_\varepsilon \\ l_\varepsilon^\varphi = \varphi, \text{ sur } \partial B_\varepsilon \end{cases} \quad (29)$$

For $v \in H^1(\Omega_\varepsilon)$, we denote by l_ε^v the harmonic function defined on B_ε such that $l_\varepsilon^v = v$ on ∂B_ε . By integration by parts $F_\varepsilon(u_0, v_\varepsilon)$ writes as

$$\begin{aligned}
F_\varepsilon(u_0, v_\varepsilon) &= - \int_{B_\varepsilon} (\nabla u_0 \cdot \nabla v_0 + \Delta u_0 v_0) - \int_{B_\varepsilon} (\nabla u_0 \cdot \nabla l_\varepsilon^{w_\varepsilon} + \Delta u_0 \cdot l_\varepsilon^{w_\varepsilon}) \\
&= - \int_{\partial B_\varepsilon} \tilde{u}_0 \partial_n v_0 + \int_{B_\varepsilon} \tilde{u}_0 \Delta v_0 - \int_{B_\varepsilon} D_u \Psi(u_0) v_0 - \int_{\partial B_\varepsilon} \tilde{u}_0 \partial_n l_\varepsilon^{w_\varepsilon} - \int_{B_\varepsilon} D_u \Psi(u_0) l_\varepsilon^{w_\varepsilon} \\
&= - \int_{\partial B_\varepsilon} \tilde{u}_0 (\partial_n v_0 + \partial_n l_\varepsilon^{w_\varepsilon}) - \int_{B_\varepsilon} D_u \Psi(u_0) v_0 + \mathcal{E}_3 + \mathcal{E}_4 \\
&= \mathcal{J}_\varepsilon + \mathcal{K}_\varepsilon + \mathcal{E}_3 + \mathcal{E}_4
\end{aligned} \tag{30}$$

with $\tilde{u}_0 = u_0 - u_0(0)$ and

$$\begin{aligned}
\mathcal{J}_\varepsilon &= - \int_{\partial B_\varepsilon} \tilde{u}_0 (\partial_n v_0 + \partial_n l_\varepsilon^{w_\varepsilon}) & \mathcal{K}_\varepsilon &= - \int_{B_\varepsilon} D_u \Psi(u_0) v_0 \\
\mathcal{E}_3 &= \int_{B_\varepsilon} \tilde{u}_0 \Delta v_0 & \mathcal{E}_4 &= - \int_{B_\varepsilon} D_u \Psi(u_0) l_\varepsilon^{w_\varepsilon}
\end{aligned} \tag{31}$$

The computation of \mathcal{J}_ε , \mathcal{E}_1 , \mathcal{E}_2 and \mathcal{E}_4 needs to approximate w_ε and $X_\varepsilon = u_\varepsilon - u_0$ in the $H^1(\Omega_\varepsilon)$ sense. From Lemma 10.3 (see Appendix A), we can show that $\|X_\varepsilon\|_{0, \Omega_\varepsilon} = O(\varepsilon^2 \sqrt{-\log(\varepsilon)})$ and that $w_\varepsilon = \varepsilon Q\left(\frac{x}{\varepsilon}\right) + r_\varepsilon$ where Q is given by (57) with $g = -\nabla v_0(0) \cdot \vec{n}$ and $\|r_\varepsilon\|_{1, \Omega_\varepsilon} = O(\varepsilon^2 \sqrt{-\log(\varepsilon)})$.

Proposition 2. *Let \mathcal{J}_ε , \mathcal{J}_ε , \mathcal{K}_ε , \mathcal{E}_1 , \mathcal{E}_2 , \mathcal{E}_3 and \mathcal{E}_4 given by (23), (28) and (31), we have the following estimations :*

$$\begin{aligned}
J_\varepsilon(u_\varepsilon) - J_0(u_0) &= \mathcal{J}_\varepsilon + \mathcal{J}_\varepsilon + \mathcal{K}_\varepsilon + \sum_{i=1}^4 \mathcal{E}_i \\
\mathcal{J}_\varepsilon &= \pi \varepsilon^2 D_u \Psi(0, u_0) u_0(0) \\
\mathcal{J}_\varepsilon &= -2\pi \varepsilon^2 \nabla u_0(0) \cdot \nabla v_0(0) \\
\mathcal{K}_\varepsilon &= -\pi \varepsilon^2 D_u \Psi(0, u_0) v_0(0)
\end{aligned} \tag{32}$$

and $\mathcal{E}_i \sim o(\varepsilon^2)$ for $i \in \llbracket 1..4 \rrbracket$

Démonstration. The first equality is straightforward. Lemma 10.3, the regularity of $\psi(x, u)$ and Proposition 1 allow to say that \mathcal{E}_1 and \mathcal{E}_2 are $O(\|u_\varepsilon - u_0\|_{0, \Omega_\varepsilon}^2)$ and then $\sim O(-\varepsilon^4 \log(\varepsilon))$. We recall the notation $\Psi(u)$ means $\Psi(x, u(x))$. A change of variable (CV) and the continuity of $x \mapsto D_u \Psi(x, u_0(x))$ lead to

$$\begin{aligned}
\mathcal{J}_\varepsilon &= \varepsilon^2 \int_B D_u \Psi(\varepsilon X, u_0(\varepsilon X)) u_0(\varepsilon X) = \varepsilon^2 \pi D_u \Psi(0, u_0) u_0(0) + o(\varepsilon^2) \\
\mathcal{K}_\varepsilon &= \varepsilon^2 \int_B D_u \Psi(\varepsilon X, u_0(\varepsilon X)) v_0(\varepsilon X) dX = \varepsilon^2 \pi D_u \Psi(0, u_0) v_0(0) + o(\varepsilon^2)
\end{aligned}$$

Again with a CV, the equality $\Delta v_0 = D_u^2 \Psi(u_0)(v_0 - u_0) - D_u \Psi(u_0)$ and the regularity of $\Psi(u)$, we get $\mathcal{E}_3 \sim O(\varepsilon^3)$. By using Lemma 10.4 and Lemma 10.1 (see Appendix A) we have :

$$\begin{aligned}
\mathcal{J}_\varepsilon &= \int_{\partial B} (u_0 - u_0(0)) (\partial_n l_\varepsilon^{l_\varepsilon^{e_\varepsilon}} + \partial_n v_0) + \int_{\partial B_\varepsilon} (u_0 - u_0(0)) \partial_n l_\varepsilon^{e_\varepsilon} \\
&= \varepsilon^2 \nabla u_0(0) \cdot \int_{\partial B} \lambda(x) x + \mathcal{F}_1 + \mathcal{F}_2
\end{aligned}$$

with

$$\begin{aligned}\lambda(x) &= -2\nabla v_0(0) \cdot \vec{n} \\ \mathcal{F}_1 &= \int_{\partial B_\varepsilon} (u_0 - u_0(0)) (\partial_n v_0 - \nabla v_0(0) \cdot \vec{n}) \\ \mathcal{F}_2 &= \int_{\partial B_\varepsilon} (u_0 - u_0(0)) \partial_n l_\varepsilon^{\varepsilon^\varepsilon}\end{aligned}$$

A CV and a Taylor expansion of u_0 and v_0 at 0 lead to $\mathcal{F}_1 = O(\varepsilon^3)$ and $\mathcal{F}_2 \leq C\varepsilon^2 \|\partial_n l_\varepsilon^{\varepsilon^\varepsilon}(\varepsilon X)\|_{-1/2, \partial B}$. For \mathcal{F}_2 it suffices to make a CV and use the trace Theorem on $B_2 \setminus \bar{B}$:

$$\begin{aligned}\|\partial_n l_\varepsilon^{\varepsilon^\varepsilon}(\varepsilon X)\|_{-1/2, \partial B} &\leq \frac{1}{\varepsilon} |l_\varepsilon^{\varepsilon^\varepsilon}(\varepsilon X)|_{1, B} = \frac{1}{\varepsilon} |l^{\varepsilon^\varepsilon(\varepsilon X)}(X)|_{1, B} \\ &\leq \frac{C}{\varepsilon} \|e_\varepsilon(\varepsilon X)\|_{H^{1/2}(\partial B)/\mathbb{R}} \leq C \|e_\varepsilon(\varepsilon X)\|_{H^1(B_2 \setminus \bar{B})/\mathbb{R}}\end{aligned}$$

Now from the equivalency of the $H^1(B_2 \setminus \bar{B})/\mathbb{R}$ -norm with the semi norm and a CV we get $\|\partial_n l_\varepsilon^{\varepsilon^\varepsilon}(\varepsilon X)\|_{-1/2, \partial B} \leq C|e_\varepsilon|_{1, \Omega_\varepsilon}$. By using Lemma 10.4, we obtain $\mathcal{F}_2 = O(\varepsilon^3 \sqrt{-\log(\varepsilon)})$. Finally by using a CV, the continuity of $\varphi \mapsto l^\varphi$ from $H^{1/2}(\partial B)$ to $H^1(B)$, the trace Theorem on $B_2 \setminus \bar{B}$, again a CV and Lemma 10.4 we have :

$$\begin{aligned}|\mathcal{E}_4| &\leq C\varepsilon^2 \|l_\varepsilon^{w_\varepsilon}(\varepsilon X)\|_{0, B} = C\varepsilon^2 \|l^{w_\varepsilon(\varepsilon X)}(X)\|_{0, B} \\ &\leq C\varepsilon^2 \|w_\varepsilon(\varepsilon X)\|_{1/2, \partial B} \leq C \|w_\varepsilon(\varepsilon X)\|_{1, B_2 \setminus \bar{B}} \\ &\leq C\varepsilon^2 \left(\frac{1}{\varepsilon} \|w_\varepsilon\|_{0, \Omega_\varepsilon} + |w_\varepsilon|_{1, \Omega_\varepsilon} \right) \leq C\varepsilon^3 \sqrt{-\log(\varepsilon)}\end{aligned}$$

□

The topological expression is easily deduced from Proposition 2 and Theorem 5.2 is proven. □

5.3 Expression of the topological gradient for a cracked domain

For the cracked domain $\Omega_\varepsilon = \Omega \setminus \overline{x_0 + \varepsilon \sigma(\vec{n})}$, computations are similar. The term \mathcal{J}_ε of (27) is zero and the term $F_\varepsilon(u_0, v_\varepsilon)$ expresses as $F_\varepsilon(u_0, v_\varepsilon) = -\int_{B_\varepsilon} \partial_n u_0 [w_\varepsilon]$. The asymptotic expansion of u_ε and v_ε are similar and then the computation of the topological gradient is the same as in the linear case (see [4, 21] for more details).

Theorem 5.3. *The topological gradient I_{Lap}^c associated to problem (19) and to the cost function $J_\varepsilon(u) = \int_{\Omega_\varepsilon} |\nabla u|^2$ for a cracked domain is*

$$\begin{aligned}I_{Lap}^c(x_0) &= \min_{\|\vec{n}\|=1} \mathcal{J}(x_0, \vec{n}) \\ &\text{with } \mathcal{J}(x_0, \vec{n}) = -\pi \nabla u_0(x_0) \cdot \vec{n} \nabla v_0(x_0) \cdot \vec{n}\end{aligned}\tag{33}$$

with u_0 and v_0 given by (19) and (26) for $\varepsilon = 0$ and with $\gamma > 0$ in front of the Laplacian.

6 Poissonian model with blurring

We recall that we model the observed image f as a step function defined by $f_j \in \mathbb{R}$ on R_j for $j \in I_{ind}(\Omega)$, where R_j is a regular domain of \mathbb{R}^2 modeling pixel j and we denote $N = |I_{ind}(\Omega)|$. To simplify, we suppose that $|R_j| = 1$ and that Ω is the disjoint union of the $(R_i)_{i \in I_{ind}(\Omega)}$. We assume that

$\min_{j \in I_{ind}(\Omega)} f_j > 0$. We recall the general minimization problem associated to the Poisson model given in (12) :

$$\min_{u \in H^1(\Omega)} \frac{\gamma}{2} J_\Omega(u) + \sum_{j \in I_{ind}(\Omega)} \psi_j \left(\int_{R_j} Ku \right) \quad (34)$$

with $\psi_j(x) = x - f_j \log(x)$. We still denote in this section $J_\Omega(u) = \int_\Omega |\nabla u|^2$ and $E_\Omega(u) = \frac{\gamma}{2} J_\Omega(u) + \sum_{j \in I_{ind}(\Omega)} \psi_j \left(\int_{R_j} Ku \right)$.

First we show that problem (34) is well-posed, then we compute the topological gradient for a perforated domain (a) : $\Omega_\varepsilon = \Omega \setminus \overline{x_0 + \varepsilon B}$, and we give the expression for a cracked domain (b) : $\Omega_\varepsilon = \Omega \setminus \overline{x_0 + \varepsilon \sigma}$ without proof.

6.1 Well-posedness of problem (34)

Proposition 3. *Let f a step function such that $\min_i f_i > 0$ and $\max_i f_i < +\infty$, then problem (34) with $\psi_j(x) = x - f_j \log(x)$ for $j \in I_{ind}(\Omega)$ admits a unique solution $u \in H^1(\Omega)$.*

Moreover this solution verifies $\alpha \leq \int_{R_i} u \leq \beta$, $\forall i \in I_{ind}(\Omega)$ with $\alpha = \frac{\min_i f_i}{N}$ and $\beta = \int_\Omega f = \sum_{i \in I_{ind}(\Omega)} f_i$.

Démonstration. Existence : To simplify the proof we suppose that K is the identity operator and $\gamma = 1$. The proof for the general case is quite similar. For more details see chapter 3 of [7].

We must add a priori to (34) the condition $\int_{R_i} u > 0$, $\forall i \in I_{ind}(\Omega)$.

We set $H = \{u \in H^1(\Omega), \int_{R_i} u > 0 \ \forall i \in I_{ind}(\Omega)\}$. Then (34) rewrites as :

$$\min_{u \in H(\Omega)} \int_\Omega |\nabla u|^2 + \sum_j \psi_j \left(\int_{R_j} u \right)$$

Let $(u_n)_n$ a minimizing sequence of $E_\Omega(u)$ in $H(\Omega)$. There exists a constant $D > 0$ such that $J_\Omega(u_n) \leq D$.

If $C = \sum_j \min_{x \in]0, +\infty[} \psi_j(x) = \sum_j f_j - f_j \log(f_j) > -\infty$, then :

$$0 \leq \int_\Omega |\nabla u_n|^2 \leq \max(D, D - C)$$

By using the positiveness of $\int_\Omega |\nabla u_n|^2$, we deduce that $\sum_j \psi_j \left(\int_{R_j} u_n \right) \leq D$. Setting $K_i = \sum_{j \neq i} \min_x \psi_j$, it is straightforward that $\psi_i \left(\int_{R_i} u_n \right) \leq D - K_i$ and then

$$0 < \underline{E}_i \leq \int_{R_i} u_n \leq \overline{E}_i \quad (35)$$

with $\overline{E}_i = \max \{ \psi_i^{-1}(D - K_i) \}$ and $\underline{E}_i = \min \{ \psi_i^{-1}(D - K_i) \}$ (we recall the notation $\psi_i^{-1}(b) = \{x \in]0, \infty[\mid \psi_i(x) = b\}$). Hence the constraint $\int_{R_i} u_n > 0$ is fulfilled. We deduce that $\sum_i \underline{E}_i \leq \int_\Omega u_n = \sum_i \int_{R_i} u_n \leq \sum_i \overline{E}_i$ and thanks to Poincaré-Wirtinger Lemma we get that u_n is bounded in $L^2(\Omega)$. So, there exist a subsequence u_{n_k} (still denoted u_n) and $u \in H^1(\Omega)$ such that $u_n \xrightarrow{L^2(\Omega)} u$ and $u_n \xrightarrow{H^1(\Omega)^*} u$. We deduce that $J_\Omega(u) \leq \liminf J_\Omega(u_n)$ and thanks to (35) and Bolzano-Weierstrass Lemma, we can extract a subsequence u_n such that $\int_{R_i} u_n \rightarrow l_i \in \mathbb{R}$. By continuity, we have $\psi_i \left(\int_{R_i} u_n \right) \rightarrow \psi_i(l_i) \ \forall i \in I_{ind}(\Omega)$ and

$$E_\Omega(u) \leq \liminf E_\Omega(u_n)$$

which proves that u is a minimizer of $E_\Omega(u)$ in $H^1(\Omega)$.

Bounds : If $u \in H^1(\Omega)$ is the solution of (34) then $DE_\Omega(u).v = 0 \quad \forall v \in H^1(\Omega)$ i.e.

$$\int_{\Omega} \nabla u \cdot \nabla v + \sum_{j \in I_{ind}(\Omega)} D\psi_j \left(\int_{R_j} u \right) \int_{R_j} v = 0, \quad \forall v \in H^1(\Omega) \quad (36)$$

with $D\psi_j \left(\int_{R_j} u \right) = 1 - \frac{f_j}{\int_{R_j} u}$.

(i) By taking $v = 1$, we get the equality $N = \sum_j \frac{f_j}{\int_{R_j} u}$. As $\frac{f_j}{\int_{R_j} u} \geq 0, \forall j \in I_{ind}(\Omega)$ and if $i_0 = \operatorname{argmin}_i \int_{R_i} u$, we have $N \geq \frac{f_{i_0}}{\int_{R_{i_0}} u}$ which leads to $\int_{R_{i_0}} u \geq \frac{f_{i_0}}{N} \geq \frac{\min_i f_i}{N}$.

(ii) By taking $v = u$, we get the inequality $\sum_i \int_{R_i} u - f_i \leq 0$ which leads to $\max_i \int_{R_i} u \leq \sum_i \int_{R_i} u \leq \sum_i f_i$.

Uniqueness : From the two previous points we can consider the minimization space

$H(\Omega) = \left\{ u \in H^1(\Omega), \alpha \leq \int_{R_j} u \leq \beta \right\}$. Since $\psi_j(X)$ is strictly convex on $[\alpha, \beta]$ for all $j \in I_{ind}(\Omega)$, we get from the linearity of the integral that $u \mapsto \psi_j \left(\int_{R_j} u \right)$ is strictly convex on $H(\Omega)$. As J_Ω is strictly convex, we deduce that $E_\Omega(u)$ is strictly convex on the convex set $H(\Omega)$ and so that E_Ω has a unique minimum in $H^1(\Omega)$. \square

Remark 4. (i) Under the same hypotheses on f , we get the existence and uniqueness of a solution u_ε in $H^1(\Omega_\varepsilon)$ for (19). For ε small enough, we still have $\min_i \int_{R_i^\varepsilon} u_\varepsilon \geq \frac{\min_i f_i}{N}$ and $\max_i \int_{R_i^\varepsilon} u_\varepsilon \leq \int_{\Omega} f = \sum_{i=1}^N f_i, \forall i \in I_{ind}(\Omega)$.

(ii) When $K \neq I$ is such that $K\mathbf{1} \neq 0$, we can show that problem (34) is well-posed in $H^1(\Omega)$. For more details we refer the reader to [7] chapter 3.

(iii) We can show that Proposition 3 holds as soon as ψ_j are bounded from below for $j \in I_{ind}(\Omega)$ and strictly convex on $I \subset \mathbb{R}$. In the general case α and β are implicitly defined in function of ψ_j .

6.2 Computation of the topological gradient for a perforated domain

In this section we compute the topological gradient for a perforated domain $\Omega_\varepsilon = \Omega \setminus \overline{\{x_0 + \varepsilon B\}}$. Let $j_0 \in I_{ind}(\Omega)$ be such that $R_{j_0} \supset B_\varepsilon(x_0)$ where $B_\varepsilon(x_0)$ is the ball centered at x_0 and of radius ε . For $j \in I_{ind}(\Omega)$, let R_j^ε be the domain equal to $R_{j_0} \setminus \overline{B_\varepsilon(x_0)}$ if $j = j_0$ and R_j otherwise. Now let us denote $I_j^\varepsilon(u) = \int_{R_j^\varepsilon} u, I_j(u) = \int_{R_j} u, J_\varepsilon(u) = J_{\Omega_\varepsilon}(u)$ and u_ε the solution of (34) replacing Ω by Ω_ε .

By writing $DE_{\Omega_\varepsilon}.v = 0 \quad \forall v \in H^1(\Omega_\varepsilon)$, we deduce the following variational formulation of (34) :

$$\text{find } u_\varepsilon \in H^1(\Omega_\varepsilon) \text{ such that } F_\varepsilon(u_\varepsilon, v) = 0 \quad \forall v \in H^1(\Omega_\varepsilon)$$

where $F_\varepsilon(u, v)$ is the following functional on $H^1(\Omega_\varepsilon) \times H^1(\Omega_\varepsilon)$:

$$F_\varepsilon(u, v) = \int_{\Omega_\varepsilon} \gamma \nabla u \cdot \nabla v + \sum_{j \in I_{ind}(\Omega)} D\psi_j \left(I_j^\varepsilon(Ku) \right) \int_{R_j^\varepsilon} Kv \quad (37)$$

By taking $v \in \mathcal{D}(R_j^\varepsilon)$, the space of $C^\infty(R_j^\varepsilon)$ functions with compact support in R_j^ε , we obtain $-\gamma \Delta u_\varepsilon + D\psi_j(I_j^\varepsilon(Ku_\varepsilon))K^*\mathbf{1} = 0$ on $R_j^\varepsilon, \forall j \in I_{ind}(\Omega)$. Then if v is any test function $v \in H^1(\Omega)$, we get $\partial_n u_\varepsilon = 0$ on $\partial\Omega_\varepsilon$. Therefore :

$$(\mathcal{P}_\varepsilon) \begin{cases} -\gamma \Delta u_\varepsilon + D\psi_j \left(I_j^\varepsilon(Ku_\varepsilon) \right) K^*\mathbf{1} = 0, & \text{on } R_j^\varepsilon \\ \partial_n u_\varepsilon = 0 & \text{on } \partial\Omega_\varepsilon \quad \text{and} \quad [u_\varepsilon]_{\partial R_j} = 0 \end{cases} \quad (38)$$

where $[u_\varepsilon]_{\partial R_j}$ denotes the jump of u_ε through ∂R_j .

We now give the main result of this section. The proof is performed in the case $\gamma = 1$ and $K = I$ but the proof is the same in the general case.

Theorem 6.1. *The topological gradient I_{Lap}^b associated to problem (38) and to the cost function $J_\varepsilon(u) = \int_{\Omega_\varepsilon} |\nabla u|^2$ for a perforated domain is*

$$\begin{aligned} I_{Lap}^b(x_0) &= -2\pi \nabla u_0(x_0) \cdot \nabla v_0(x_0) + \frac{\pi}{\gamma} D\psi_{j_0}(I_{j_0}(Ku_0))(Ku_0(x_0) - Kv_0(x_0)) \\ &\quad + \frac{\pi}{\gamma} D^2\psi_{j_0}(I_{j_0}(Ku_0))Ku_0(x_0)(I_{j_0}(Ku_0) - I_{j_0}(Kv_0)) \end{aligned} \quad (39)$$

with u_0 and v_0 given by (38) and (44) for $\varepsilon = 0$.

Démonstration. We set

$$\tilde{J}_\varepsilon(u) = - \sum_{j \in I_{ind}(\Omega)} \int_{R_j^\varepsilon} D\psi_j(I_j^\varepsilon(u)) u = - \sum_{j \in I_{ind}(\Omega)} D\psi_j(I_j^\varepsilon(u)) I_j^\varepsilon(u)$$

The difference $J_\varepsilon(u_\varepsilon) - J_0(u_0)$ is :

$$J_\varepsilon(u_\varepsilon) - J_0(u_0) = \tilde{J}_\varepsilon(u_\varepsilon) - \tilde{J}_\varepsilon(u_0) = L_\varepsilon(u_\varepsilon - u_0) + \mathcal{J}_\varepsilon \quad (40)$$

with

$$\begin{aligned} L_\varepsilon(u) &= - \sum_{j \in I_{ind}(\Omega)} \int_{R_j^\varepsilon} (D\psi_{j_0}(I_{j_0}(u_0)) + D^2\psi_{j_0}(I_{j_0}(u_0))I_{j_0}(u_0)) u \\ &= - \sum_{j \in I_{ind}(\Omega)} \int_{R_j^\varepsilon} u \\ \mathcal{J}_\varepsilon &= \int_{B_\varepsilon} (D\psi_{j_0}(I_{j_0}(u_0)) + D^2\psi_{j_0}(I_{j_0}(u_0))I_{j_0}(u_0)) u_0 \\ &= \int_{B_\varepsilon} u_0 \end{aligned} \quad (41)$$

Then in order to introduce the adjoint problem, we make a second order Taylor expansion with respect to u for $F_\varepsilon(u, v)$:

$$F_\varepsilon(u_\varepsilon, v) = G_\varepsilon(u_0, v) + b_\varepsilon(u_\varepsilon - u_0, v) + c_\varepsilon(v) + d_\varepsilon(v) \quad (42)$$

with

$$\begin{aligned} G_\varepsilon(u, v) &= \int_{\Omega_\varepsilon} \nabla u \cdot \nabla v + \sum_{j \in P(\Omega)} D\psi_j(I_j(u)) \int_{R_j^\varepsilon} v \\ b_\varepsilon(u, v) &= \int_{\Omega_\varepsilon} \nabla u \cdot \nabla v + \sum_{j \in I_{ind}(\Omega)} D^2\psi_j(I_j(u_0)) \int_{R_j^\varepsilon} u \int_{R_j^\varepsilon} v \\ c_\varepsilon(v) &= \frac{1}{2} \sum_{j \in I_{ind}(\Omega)} \int_{R_j^\varepsilon} D^3\psi_j(\xi_\varepsilon) (I_j^\varepsilon(u_\varepsilon) - I_j^0(u_0))^2 \int_{R_j^\varepsilon} v \\ d_\varepsilon(v) &= -D^2\psi_{j_0}(I_{j_0}(u_0)) \int_{B_\varepsilon} u_0 \int_{R_{j_0}^\varepsilon} v \end{aligned}$$

where $\xi_\varepsilon = \theta \int_{R_j^\varepsilon} u_\varepsilon + (1 - \theta) \int_{R_j} u_0 \in [\alpha, \beta]$ with $0 < \theta < 1$. Next, we introduce the adjoint problem : find $v_\varepsilon \in H^1(\Omega_\varepsilon)$ solution of

$$b_\varepsilon(u, v_\varepsilon) = -L_\varepsilon(u) \quad \forall u \in H^1(\Omega_\varepsilon) \quad (43)$$

By taking $u \in \mathcal{D}(R_j^\varepsilon)$ and by integrating by parts, we deduce the following Euler equations associated with (43)

$$\begin{cases} -\Delta v_\varepsilon + D^2 \psi_j(I_j(u_0)) \int_{R_j^\varepsilon} v_\varepsilon = \mathbf{1} \text{ on } R_j^\varepsilon \\ \partial_n v_\varepsilon = 0 \text{ on } \partial\Omega_\varepsilon \quad \text{and} \quad [v_\varepsilon]_{\partial R_j} = 0 \end{cases}$$

Remark 5. For $\gamma \neq 1$ and $K \neq I$, the adjoint problem is defined by

$$\begin{cases} -\gamma \Delta v_\varepsilon + D^2 \psi_j(I_j(Ku_0)) \int_{R_j^\varepsilon} K v_\varepsilon = K^* \mathbf{1} \text{ on } R_j^\varepsilon \\ \partial_n v_\varepsilon = 0 \text{ on } \partial\Omega_\varepsilon \quad \text{and} \quad [v_\varepsilon]_{\partial R_j} = 0 \end{cases} \quad (44)$$

From (40) and (42), we obtain

$$\begin{aligned} J_\varepsilon(u_\varepsilon) - J_0(u_0) &= -L_\varepsilon(u_\varepsilon - u_0) + \mathcal{J}_\varepsilon = -b_\varepsilon(u_\varepsilon - u_0, v_\varepsilon) + \mathcal{J}_\varepsilon \\ &= G_\varepsilon(u_0, v_\varepsilon) + c_\varepsilon(v_\varepsilon) + d_\varepsilon(v_\varepsilon) + \mathcal{J}_\varepsilon \\ &= G_\varepsilon(u_0, v_\varepsilon) + \mathcal{J}_\varepsilon + \mathcal{E}_1 \end{aligned} \quad (45)$$

with

$$\mathcal{E}_1 = c_\varepsilon(v_\varepsilon) \quad \text{and} \quad \mathcal{J}_\varepsilon = d_\varepsilon(v_\varepsilon) \quad (46)$$

By using an integration by parts, $G_\varepsilon(u_0, v_\varepsilon)$ expresses as

$$\begin{aligned} G_\varepsilon(u_0, v_\varepsilon) &= - \int_{\partial B_\varepsilon} \partial_n u_0 v_\varepsilon - \int_{\Omega_\varepsilon} \Delta u_0 v_\varepsilon + \sum_{j \in I_{\text{ind}}(\Omega)} D\psi_j(I_j(u_0)) \int_{R_j^\varepsilon} v_\varepsilon \\ &= - \int_{\partial B_\varepsilon} \partial_n u_0 v_\varepsilon \end{aligned}$$

With a similar computation to the one made in (30) for the speckle model, $G_\varepsilon(u_0, v_\varepsilon)$ rewrites as :

$$\begin{aligned} G_\varepsilon(u_0, v_\varepsilon) &= - \int_{\partial B_\varepsilon} \tilde{u}_0 (\partial_n v_0 + \partial_n l_\varepsilon^{w_\varepsilon}) - D\psi_{j_0}(I_{j_0}(u_0)) \int_{B_\varepsilon} v_0 + \int_{B_\varepsilon} \tilde{u}_0 \Delta v_0 - D\psi_{j_0}(I_{j_0}(u_0)) \int_{B_\varepsilon} l_\varepsilon^{w_\varepsilon} \\ &= \mathcal{H}_\varepsilon + \mathcal{L}_\varepsilon + \mathcal{E}_2 + \mathcal{E}_3 \end{aligned}$$

with $\tilde{u}_0 = u_0 - u_0(0)$, $w_\varepsilon = v_\varepsilon - v_0$ and

$$\begin{aligned} \mathcal{H}_\varepsilon &= - \int_{\partial B_\varepsilon} \tilde{u}_0 (\partial_n v_0 + \partial_n l_\varepsilon^{w_\varepsilon}) \\ \mathcal{L}_\varepsilon &= -D\psi_{j_0}(I_{j_0}(u_0)) \int_{B_\varepsilon} v_0 \\ \mathcal{E}_2 &= \int_{B_\varepsilon} \tilde{u}_0 \Delta v_0 \quad , \quad \mathcal{E}_3 = -D\psi_{j_0}(I_{j_0}(u_0)) \int_{B_\varepsilon} l_\varepsilon^{w_\varepsilon} \end{aligned} \quad (47)$$

In the following proposition we give the asymptotic expansion of the previous quantities.

Proposition 4. Let \mathcal{I}_ε , \mathcal{J}_ε , \mathcal{K}_ε , \mathcal{L}_ε , \mathcal{E}_1 , \mathcal{E}_2 and \mathcal{E}_3 given by (41), (46) and (47), then we have the following estimations :

$$\begin{aligned}
J_\varepsilon(u_\varepsilon) - J_0(u_0) &= \mathcal{I}_\varepsilon + \mathcal{J}_\varepsilon + \mathcal{K}_\varepsilon + \mathcal{L}_\varepsilon + \sum_{i=1}^3 \mathcal{E}_i \\
\mathcal{I}_\varepsilon &= \pi\varepsilon^2 (D\psi_{j_0}(I_{j_0}(u_0)) + D^2\psi_{j_0}(I_{j_0}(u_0))I_{j_0}(u_0))u_0(0) + o(\varepsilon^2) \\
\mathcal{J}_\varepsilon &= -\pi\varepsilon^2 D^2\psi_{j_0}(I_{j_0}(u_0))u_0(0)I_{j_0}(v_0) + o(\varepsilon^2) \\
\mathcal{K}_\varepsilon &= -2\pi\varepsilon^2 \nabla u_0(0) \cdot \nabla v_0(0) + o(\varepsilon^2) \\
\mathcal{L}_\varepsilon &= -\pi\varepsilon^2 D\psi_{j_0}(I_{j_0}(u_0))v_0(0) + o(\varepsilon^2)
\end{aligned} \tag{48}$$

and $\mathcal{E}_i \sim o(\varepsilon^2)$ for $i \in \{1, 2, 3\}$.

Démonstration. The first equality is straightforward. A Taylor expansion of u_0 at 0 gives the first estimation. Again a Taylor expansion of u_0 at 0, Lemma 10.6 (see Appendix B) and the fact that $R_{j_0}^\varepsilon \xrightarrow{\varepsilon \rightarrow 0} R_{j_0}$ give the second estimation. For \mathcal{K}_ε we refer the reader to the proof of Proposition 2. For \mathcal{E}_1 , we use Lemma 10.5, the regularity of $\psi(x)$ and that $\xi_\varepsilon \in [\alpha, \beta]$:

$$\begin{aligned}
|\mathcal{E}_1| &\leq C \sum_{j \in \mathcal{V}} \left(\int_{R_j^\varepsilon} u_\varepsilon - u_0 \right)^2 + C \left(\int_{B_\varepsilon} u_0 \right)^2 \\
&\leq C \|u_\varepsilon - u_0\|_{0, \Omega_\varepsilon}^2 + C\varepsilon^4 = O(\varepsilon^4 \log(\varepsilon))
\end{aligned}$$

By using that $\Delta v_0 = D^2\psi_{j_0}(I_{j_0}(u_0))I_{j_0}(v_0)$ and a Taylor expansion of u_0 at 0 we get $\mathcal{E}_2 = O(\varepsilon^3)$. For \mathcal{E}_3 , from a change of variable and Lemma 10.6, we get

$$|\mathcal{E}_3| \leq C\varepsilon^2 \|l_\varepsilon^{w_\varepsilon}(\varepsilon X)\|_{0, B} \leq C\varepsilon^3 \sqrt{-\log(\varepsilon)}$$

(see Proposition 2). □

Denoting by j_0 the integer such that $R_{j_0} \ni x_0$, we deduce the expression given in Theorem 6.1. □

6.3 Expression of the topological gradient for a cracked domain

For a cracked domain $\Omega_\varepsilon = \Omega \setminus \overline{\{x_0 + \varepsilon\sigma(\vec{n})\}}$, the computations are similar. The term \mathcal{I}_ε of (45) is zero and the term $F_\varepsilon(u_0, v_\varepsilon)$ expresses as $F_\varepsilon(u_0, v_\varepsilon) = -\int_{\sigma_\varepsilon} \partial_n u_0[w_\varepsilon]$. The topological expansion of u_ε and v_ε are similar with the perforated domain and the computation of the topological gradient is the same as the linear case (see [4, 21] for more details).

Theorem 6.2. *The topological gradient I_{Lap}^c associated to problem (38) and to the cost function $J_\varepsilon(u) = \int_{\Omega_\varepsilon} |\nabla u|^2$ for a cracked domain is*

$$\begin{aligned}
I_{Lap}^c(x_0) &= \min_{|\vec{n}|=1} \mathcal{I}(x_0, \vec{n}) \\
\text{with } \mathcal{I}(x_0, \vec{n}) &= -\pi \nabla u_0(x_0) \cdot \vec{n} \nabla v_0(x_0) \cdot \vec{n}
\end{aligned} \tag{49}$$

with u_0 and v_0 given by (38) and (44) for $\varepsilon = 0$.

Remark 6. The topological gradient is the same in the general case of functions $\psi_j \in C^3(I)$, strictly convex on I and bounded from below on I . Just in the right hand-side of (44), $K^*\mathbb{1}$ must be replaced by $(D^2\psi_j(I_j(Ku_0))I_j(Ku_0) + D\psi_j(I_j(Ku_0)))K^*\mathbb{1}$.

7 Summary table of the topological gradient expressions

We summarize in Table 1, all the expressions of the topological gradient according to the type of noise and to the infinitesimal perturbation.

	Ball	Crack
Gauss ($K \neq I$)	$-2\pi \nabla u_0(x_0) \cdot \nabla v_0(x_0) + \frac{\pi}{\gamma} (f(x_0) - Ku_0(x_0))(Kv_0(x_0) - Ku_0(x_0))$	$-\pi \nabla u_0(x_0) \cdot \vec{n} \nabla v_0(x_0) \cdot \vec{n}$
Speckle-Log ($K = I$)	$-2\pi \nabla u_0(x_0) \cdot \nabla v_0(x_0) + \frac{\pi}{\gamma} D_u \psi(x_0, u_0)(u_0(x_0) - v_0(x_0))$ with $\psi(x, u) = u - \text{Log}(f(x)) + f(x)e^{-u}$	$-\pi \nabla u_0(x_0) \cdot \vec{n} \nabla v_0(x_0) \cdot \vec{n}$
Poisson ($K \neq I$)	$-2\pi \nabla u_0(x_0) \cdot \nabla v_0(x_0) + \frac{\pi}{\gamma} D \psi_{j_0}(I_{j_0}(Ku_0))(Ku_0(x_0) - Kv_0(x_0))$ $+ \frac{\pi}{\gamma} D^2 \psi_{j_0}(I_{j_0}(Ku_0)) Ku_0(x_0)(I_{j_0}(Ku_0) - I_{j_0}(Kv_0))$ with $\psi_{j_0}(x) = x - f_{j_0} \text{Log}(x)$ and $I_{j_0}(v) = \int_{R_{j_0}} v$, where $R_{j_0} \ni x_0$	$-\pi \nabla u_0(x_0) \cdot \vec{n} \nabla v_0(x_0) \cdot \vec{n}$

TABLE 1 – Summary of the topological gradient expressions

8 Restoration using the topological gradient for a cracked domain

As a by product the computation of the topological gradient I_{Lap}^c for a cracked domain allows to restore images degraded by blur or/and various noise statistics. Once I_{Lap}^c is computed, we define for a fixed threshold $\delta > 0$, the set $E_\delta = \{x \in \Omega; |I_{Lap}^c(x)| \geq \delta\}$ and the approximated characteristic function

$$\chi_\eta(x) = \begin{cases} \eta & \text{if } x \in E_\eta \\ 1 & \text{otherwise} \end{cases}$$

where η is a small positive parameter. From the computation of I_{Lap}^c we also get the normalized direction $\vec{\tau} = \vec{n}^\perp$ of the edge. If $n = (\cos(\varphi), \sin(\varphi))$ is the normal to the crack given by I_{Lap}^c , we have $\vec{\tau} = (\sin(\varphi), -\cos(\varphi))$. Then, if f is the degraded observed image, we want to find a restored version u of f as the solution of the following anisotropic PDE :

$$\begin{cases} -\text{div}(\gamma P_\eta^\varphi(x) \nabla u) + K^* D \psi(Ku) = 0 & \text{on } \Omega \\ \partial_n u = 0 & \text{on } \Gamma \end{cases} \quad (50)$$

with

$$\psi(x, u) = \begin{cases} \frac{1}{2}(f - u)^2 & \text{(Gaussian model)} \\ \sum_{j \in I_{ind}} \left(\int_{R_j} u - f_j \log \left(\int_{R_j} u \right) \right) \mathbb{1}_{R_j}(x) & \text{(Poisson model)} \\ \log(u) + \frac{f}{u} & \text{(Speckle model)} \end{cases} \quad (51)$$

and where $P_\eta^\varphi(x)$ is a tensor constructed from $\varphi(x)$ and $\chi_\eta(x)$ and γ is a parameter to tune. More precisely, we choose $P_\eta^\varphi(x) \nabla u(x) = (\nabla u \cdot \vec{\tau}) \vec{\tau} + \chi_\eta(x) (\nabla u \cdot \vec{n}) \vec{n}$. A simple identification shows that $P_\eta^\varphi(x)$ is the matrix

$$P_\eta^\varphi(x) = \begin{pmatrix} n_2^2 + \chi_\eta(x) n_1^2 & n_1 n_2 (\chi_\eta(x) - 1) \\ n_1 n_2 (\chi_\eta(x) - 1) & n_1^2 + \chi_\eta(x) n_2^2 \end{pmatrix} \quad (52)$$

where $n_1 = \cos(\varphi(x))$ and $n_2 = \sin(\varphi(x))$. The interpretation of this matrix $P_\eta^\varphi(x)$ is as follows :

- (i) if x belongs to the background, thanks to the definition of $\chi_\eta(x)$, $P_\eta^\varphi(x)$ writes as $P_\eta^\varphi(x) = I$, so $\text{div}(P_\eta^\varphi(x) \nabla u) = \Delta u$ and the smoothing is isotropic.
- (ii) if x belongs to an edge (i.e. $x \in E_\delta$), then $\chi_\eta(x)$ is close to zero and $P_\eta^\varphi(x) \nabla u(x) \approx (\nabla u \cdot \vec{\tau}) \vec{\tau}$ and the diffusion is in the direction of the edge. As we will see in section 9 on numerical examples, the restoration results obtained when applying equation (50) are very good.

9 Numerical application to 2D imaging

In this section we illustrate the theory of the topological gradient by giving various experimental results for models (13), (17) and (34).

The topological gradient expressions for the three models are stated in section 4, 5 and 6 and are summarized in section 7.

For each model, to compute the topological gradient (TG) we use Algorithm 1. The computation of the direct and adjoint solutions is specific to each model. The topological gradients are summarized in Table 1.

Algorithm 1 Computation of the topological gradient

- 1: Computation of u_0 and v_0 by using either Algorithm 2 or 3 according to the model.
 - 2: Computation of the derivatives of u_0 by convolution with derivative filters.
 - 3: Computation of the TG relatively to the model by using Table 1 and/or Theorems of section 4, 5 and 6.
-

Remark 7. For a cracked domain, indicators I_{Lap}^c (16b), (33) and (49) are given by the minimal eigenvalue of a 2×2 symmetric matrix :

$$I_{Lap}^c = \lambda_{min}(M_0)$$

with

$$M_0 = -\pi \nabla u_0 \nabla v_0^T$$

First, since equations (14) and (15) are linear, we develop the numerical analysis in a specific subsection. Then we perform the discretization of problems (17) and (34) and finally we give the experimental results. As the adjoint problems (26) and (44) are linear with non constant coefficients we discretize them by a finite difference scheme and we compute the discrete solution by using a sparse solver.

9.1 Numerical analysis for Gaussian model with blurring

To discretize (14) and (15) we use a DCT1 (discrete cosine transform of type 1) thanks to the symmetry properties and the fact that the DCT1 of a convolution product of two vectors is the product of the DCT1 of each vector. We choose this discretization because of the symmetry properties guaranteed by the algorithm. A DCT1 of N points is equivalent to a DFT (discrete Fourier transform) of $2N-2$ points. For example in 1D for $N = 4$ a DCT1 of $[x_0, x_1, x_2, x_3]$ is equivalent to a DFT of $[x_0, x_1, x_2, x_3, x_2, x_1]$. We use the FFT (fast Fourier transform) to perform the DFT. The computation time of a FFT is a $\mathcal{O}(N \log(N))$. A numerical study shows that for $N \leq 10^{10}$, FFT is faster than a finite difference scheme. Algorithm 2 gives the different steps to compute the discrete solutions (14) and (15).

It consists in the following steps :

- Symmetric extension of the initial $N_y \times N_x$ image in an $2(N_y - 1) \times 2(N_x - 1)$ image and extension of the $2n_y + 1 \times 2n_x + 1$ kernel in a $2(N_y - 1) \times 2(N_x - 1)$ kernel. To fix ideas in 1D and for $n_x = 2$, the extension of the discrete kernel $[x_{-2} x_{-1} x_0 x_1 x_2]$ is $[x_0 x_1 x_2 0 \dots 0 x_{-2} x_{-1}]$.
- Computation of the DFT of the image and of the kernels.
- Algebraic inversion in the Fourier domain.
- Computation of the solution by inverse FFT.

An important point is the choice of the frequency domain. Indeed the natural definition of the frequency domain would be $\{0, \frac{2\pi}{N_x}, \dots, \frac{2\pi(N_x-1)}{N_x}\} \times \{0, \frac{2\pi}{N_y}, \dots, \frac{2\pi(N_y-1)}{N_y}\}$, but it is not a good choice. This fact is explained in [26]. Let us give the reasoning in 1D for a 1-periodic function. The trigonometric function associated with the vector of DFT coefficients is

$$u^N(x) = \sum_{k=0}^{N-1} \widehat{y}_k^N e^{\frac{2\pi i}{N}(k+m_k N)}$$

where $\widehat{y}^N \in \mathbb{R}^N$ is the vector such that $\widehat{y}^N = \text{DFT}(y^N)$, $y^N = (u^N(l/N))_{0 \leq l \leq N-1}$ and $m_k \in \mathbb{Z}$ are coefficients which do not change function u at points $x_l = \frac{l}{N}$, but they greatly modify u between these points (aliasing phenomenon appears). If we compute the $L^2(0,1)$ -norm of the first derivative, we get :

$$\|u^N\|_{L^2(0,1)}^2 = (2\pi)^2 \sum_{k=0}^{N-1} |\widehat{y}_k^N|^2 (k + m_k N)^2 \quad (53)$$

From (53), we see that the m_k coefficients change considerably the $L^2(0,1)$ -norm of the first derivative and the good choice for m_k is the value minimizing $(k + m_k N)^2$. If $0 \leq k < N/2$ then $(k + m_k N)^2$ is minimized for $m_k = 0$ and if $N/2 \leq k < N$ then $(k + m_k N)^2$ is minimized for $m_k = -1$. A special consideration is made for $k = N/2$ when N is even because of the two possible choices ($m_k = -1$ or $m_k = 0$, see [26] for more details). By following these considerations we define the frequency domain $E = \left\{ \left(\frac{\pi k_x}{(N_x-1)}, \frac{\pi k_y}{(N_y-1)} \right), (k_x, k_y) \in E_x \times E_y \right\}$, with $E_x = \{0, \dots, N_x - 1, -(N_x - 2), \dots, -1\}$ and

$E_y = \{0, \dots, N_y - 1, -(N_y - 2), \dots, -1\}$. We denote by $\Lambda = (\Lambda_x, \Lambda_y)$ the $2(N_y - 1) \times 2(N_x - 1)$ mesh grid associated to this discrete space. The vector of Fourier coefficients associated to a discrete signal $x \in \mathbb{R}^N$ is denoted by X .

Algorithm 2 Computation of the direct and adjoint solutions

1. Given an image f_{ij} defined for $(i, j) \in \llbracket 0, N_y - 1 \rrbracket \times \llbracket 0, N_x - 1 \rrbracket$, extend it to a periodic and symmetric image defined on $\llbracket 0, 2(N_y - 1) - 1 \rrbracket \times \llbracket 0, 2(N_x - 1) - 1 \rrbracket$.
 2. Given a blurring convolution kernel k_{ij}^1 defined for $(i, j) \in \llbracket 0, 2n_y \rrbracket \times \llbracket 0, 2n_x \rrbracket$, use the procedure described in section 9.1 to calculate its symmetric extension k_{mn} for $0 \leq m < 2(N_y - 1)$ and $0 \leq n < 2(N_x - 1)$.
 3. Use an FFT to compute F_{kl} and K_{kl} for $(k, l) \in \llbracket 0, 2(N_y - 1) - 1 \rrbracket \times \llbracket 0, 2(N_x - 1) - 1 \rrbracket$.
 4. Given $\Lambda = (\Lambda_x, \Lambda_y)$, the meshgrid associated to the frequencies domain described in section 9.1, compute

$$U_{kl} = \frac{\overline{K_{kl}} F_{kl}}{|K_{kl}|^2 + \gamma \Lambda_{kl}^2} \text{ and } V_{kl} = \frac{\overline{K_{kl}} (2K_{kl} U_{kl} - F_{kl})}{|K_{kl}|^2 + \gamma \Lambda_{kl}^2}.$$
 5. Use an inverse FFT to compute u_{ij} and v_{ij} for $(i, j) \in \llbracket 0, 2(N_y - 1) - 1 \rrbracket \times \llbracket 0, 2(N_x - 1) - 1 \rrbracket$.
-

9.2 Numerical analysis for Poisson and Speckle models

If $\text{Inf}_\Omega f > 0$, by Proposition 1 and Proposition 3, problems (17) and (34) are well-posed and can be discretized as :

$$\text{(Speckle-Log model)} \quad \min_{x \geq \log(\alpha_s)} J_s(x), \quad \alpha_s > 0 \quad (54a)$$

$$\text{(Poisson model)} \quad \min_{x \geq \alpha_p} J_p(x), \quad \alpha_p > 0 \quad (54b)$$

where $\alpha_s = \min(f^N) > 0$ and $\alpha_p = \frac{\min(f^N)}{N}$. f^N is a discretization of f ; $J_p(x)$ and $J_s(x)$ are respectively the discrete versions of the energy functions (12) and (8). We choose a simple discretization : $u^N(x)$ is the step function equals to $u(j)$ on pixel j , and we represent u^N by a vector of \mathbb{R}^N .

During the construction of the sequence $x^{(k)}$, the condition $x^{(k)} \geq \alpha_p$ for the Poisson model (respectively $x^{(k)} \geq \log(\alpha_s)$ for the speckle model) must be fulfilled at each step. Hence a projection ensures this condition. To solve these problems we use an iterative algorithm based on the descent method called the SGP algorithm [17] (scaled gradient projection). Let us write the discrete cost functions :

$$J_p(x) = -\frac{\gamma}{2} x^T A x + \sum_{i=1}^N (Kx)_i - f_i \log((Kx)_i)$$

$$J_s(x) = -\frac{\gamma}{2} x^T A x + \sum_{i=1}^N \left(u_i - g_i + e^{-(u_i - g_i)} \right)$$

where A is the Neumann Laplacian matrix, K is a discretization of the blurring operator (circulant block matrix if we assume that the image is periodic) and we recall that $g_i = \log(f_i)$. Let us give the main ideas of the SGP algorithm. The discrete energies J_p and J_s are denoted by J as soon as we

do not use their expression and δ will be the number equal to α for the Poisson model and equal to $\log(\alpha)$ for the Speckle-Log model. We set $\Lambda = \{x \in \mathbb{R}^N, x \geq \delta\}$. We want to find $x^* \in \Lambda$ such that $\nabla J(x^*) = 0$. At step k , a first order Taylor expansion at point $x = x^{(k)}$ leads to the following equation

$$\nabla J(x^{(k)}) + \nabla^2 J(x^{(k)})(x - x^{(k)}) = 0$$

If $\det(\nabla^2 J(x^{(k)})) \neq 0$, we get $x = x^{(k)} - \nabla^2 J(x^{(k)})^{-1} \nabla J(x^{(k)})$. We deduce by this reasoning that the direction of the descent algorithm can be given by $\nabla^2 J(x^{(k)})^{-1} \nabla J(x^{(k)})$, but we see that the computation of this direction is very costly. We denote by \mathcal{D}_L the compact set of the symmetric positive definite $N \times N$ matrices such that $\|D\| \leq L$ and $\|D^{-1}\| \leq \frac{1}{L}$. The main idea of the SGP algorithm is to construct two sequences α_k and $D_k \in \mathcal{D}_L$ such that $\alpha_k D_k$ approximates $\nabla^2 J(x^{(k)})$ and to project each iterate on Λ with respect to the norm $\|x\|_D = \sqrt{x^T D x}$. We set $P_{\Lambda, D^{-1}}$ for $D \in \mathcal{D}_L$ the projector on Λ with respect to the norm $\|\cdot\|_D$.

We recall the SGP algorithm in Algorithm 3 (see [17]).

Algorithm 3 SGP algorithm

- 1: Set $x^{(0)} \geq \alpha$, $\beta, \theta \in]0, 1[$, $0 < \alpha_{min} < \alpha_{max}$, $L > 0$, and fix a positive integer M .
 - 2: **for** $k = 0 : k_{max}$ **do**
 - 3: Choose the parameter $\alpha_k \in [\alpha_{min}, \alpha_{max}]$ and the scaling matrix $D_k \in \mathcal{D}_L$
 - 4: Projection : $y^{(k)} \leftarrow P_{\Lambda, D_k^{-1}}(x^{(k)} - \alpha_k D_k \nabla f(x^{(k)}))$
 - 5: **if** $y^{(k)} = x^{(k)}$ **then**
 - 6: Stop, $x^{(k)}$ is a stationary point.
 - 7: **end if**
 - 8: Descent direction $d^{(k)} = y^{(k)} - x^{(k)}$;
 - 9: $\lambda_k \leftarrow 1$ and $J_{max} \leftarrow \max_{0 \leq j \leq \min(k, M-1)} J(x^{(k-j)})$
 - 10: λ_k fixed by backtracking :
 - 11: **while** $f(x^{(k)} + \lambda_k d^{(k)}) \leq J_{max} + \beta \lambda_k \nabla J(x^{(k)})^T d^{(k)}$ **do**
 - 12: $\lambda_k \leftarrow \theta \lambda_k$
 - 13: **end while**
 - 14: $x^{(k+1)} \leftarrow x^{(k)} + \lambda_k d^{(k)}$
 - 15: **end for**
-

The construction of the sequences D_k and α_k needs some explanations. We choose $D_k = \text{diag}(d_i^k)$ with $d_i^k = \min\left(L, \max\left(\frac{1}{L}, \frac{\partial^2 J}{\partial x_i^2}(x^{(k)})^{-1}\right)\right)$. The approximation of the Hessian matrix $\nabla^2 J(x^{(k)})$ is $B(\alpha_k) = \alpha_k D_k$. By using a first order Taylor expansion of $\nabla J(x)$ at point $x^{(k-1)}$ we get that

$$\nabla J(x^{(k)}) - \nabla J(x^{(k-1)}) = \nabla^2 J(x^{(k)}).(x^{(k)} - x^{(k-1)}) + o\left((x^{(k)} - x^{(k-1)})^2\right)$$

Hence two possible choices of α_k can be made :

$$\alpha_k^1 = \arg \min_{\alpha} \left\| B(\alpha_k) s^{(k-1)} - z^{(k-1)} \right\|_{D_k} = \frac{s^{(k-1)T} D_k^{-1} D_k^{-1} s^{(k-1)}}{s^{(k-1)T} D_k^{-1} z^{(k-1)}}$$

$$\alpha_k^2 = \arg \min_{\alpha} \left\| s^{(k-1)} - B(\alpha_k)^{-1} z^{(k-1)} \right\|_{D_k} = \frac{s^{(k-1)T} D_k z^{(k-1)}}{z^{(k-1)T} D_k D_k z^{(k-1)}}$$

where $s^{(k-1)} = x^{(k)} - x^{(k-1)}$ and $z^{(k-1)} = \nabla J(x^{(k)}) - \nabla J(x^{(k-1)})$. In [17] the choice of α_k is the output of an algorithm called SGP-SS Algorithm (SGP step length selection) which uses two thresholds $0 < \alpha_{min} < \alpha_{max}$. Let us give the derivative of the discrete cost functions J_p and J_s :

$$\begin{aligned}\nabla J_p &= -\gamma Ax - K^T \frac{f}{Kx} + K^T \mathbb{1} \\ \nabla^2 J_p &= -\gamma A + K^T \text{diag} \left(\frac{f}{(Kx)^2} \right) K \\ \nabla J_s &= -\gamma Ax + 1 - e^{-(x-f)} \\ \nabla^2 J_s &= -\gamma A + \text{diag} \left(e^{-(x-f)} \right)\end{aligned}$$

where $\mathbb{1} \in \mathbb{R}^N$ denotes the vector with each coefficient equal to 1, $\text{diag}(x)$ for $x \in \mathbb{R}^N$ is the diagonal matrix with diagonal entries equal to x . For $x \in \mathbb{R}^N$ and $\varphi : \mathbb{R} \rightarrow \mathbb{R}$ a function, $\varphi(x)$ stands for the vector $(\varphi(x_i))_{1 \leq i \leq N}$. The choice of the parameters in Algorithm 3 is the following : $\beta = 10^{-4}$, $\theta = 0.4$, $k_{max} = 600$, $M = 1$ and for the Poisson model (34) we set $\alpha_{min} = 10^{-10}$, $\alpha_{max} = 10^5$ while for the Speckle-Log model (17) we set $\alpha_{min} = 10^{-5}$, $\alpha_{max} = 10^{15}$. The initial value of $x^{(0)}$ is either the observed image for the Poisson model or its logarithm for the Speckle-Log model. Let us note that in the case of the speckle model, (50) is performed with $\psi(u) = \log(u) + \frac{f}{u}$.

9.3 Comparison of our method with some classical models

As said in the introduction other variational methods exist for segmenting/restoring images.

We will compare the topological gradient segmentation process with the one performed by the Mumford-Shah model. We will also compare the restoration proposed in (50) with the ones given by the Mumford-Shah restoration and by the TV restoration.

Mumford-Shah model of segmentation/restoration and its approximation

Let u the image of support Ω , the functional introduced by Mumford and Shah in 1989 (see [33]) is :

$$F(u, \gamma) = \int_{\Omega} |u - u_0|^2 + \lambda \int_{\Omega \setminus \bar{\gamma}} |\nabla u|^2 + \alpha \mathcal{H}^1(\gamma)$$

where f is the observed image, u is a function defined on $\Omega \setminus \bar{\gamma}$ (the restored version of f) and $\gamma \subset \Omega$ is the set of discontinuity of u . \mathcal{H}^1 is the Hausdorff measure of γ , λ and α are positive parameters. The difficulty was that the unknown are not of same nature : u is a function and γ is a set. Ambrosio and Tortorelli [1] proposed an approximation of this functional as follows :

$$\mathcal{F}_{\varepsilon}(u, b) = \int_{\Omega} \left[|u - f|^2 + \lambda b^2 |\nabla u|^2 + \alpha \left(\varepsilon |\nabla b|^2 + \frac{(b-1)^2}{4\varepsilon} \right) \right]$$

We will change the data fidelity term $|u - f|^2$ according to the a priori model (Gaussian, Poissonian and speckle model) i.e. the model that we will compare with (50) is (see [35]) :

$$\min_{u \in H^1(\Omega), b \in H^1(\Omega)} \int_{\Omega} \left[\psi(x, Ku) + \lambda b^2 |\nabla u|^2 + \alpha \left(\varepsilon |\nabla b|^2 + \frac{(b-1)^2}{4\varepsilon} \right) \right] \quad (55)$$

where K is the blur operator, $u(x)$ is the restored image, $1 - b(x) \approx 0$ is the characteristic function of the edges and $\psi(x, u)$ is given in (51). We will call this model the Mumford-Shah model (MS).

TV model of restoration

The TV model is well-known : we search for a restored version u minimizing an energy functional which is the sum of the total variation $\|Du\|$ and a data fidelity term which depends on the a priori model (see [8] for the speckle model and [16] for the Poisson one). Thus, we will compare our model (50) to :

$$\min_{u \in \mathcal{BV}(\Omega)} \int_{\Omega} |Du| + \lambda \psi(x, Ku) \quad (56)$$

where λ is a parameter, K the blur operator, and $\psi(u)$ is given in (51). In the sequel we call this model the TV model.

For more details on these models we refer the reader to [16], [8], [35] and [33].

For restoration comparisons on synthetic images we use two indicators :

- the PSNR which is defined for a noisy observation I of an image I_0 by

$$PSNR(I) = 10 \text{Log} \left(\frac{255^2}{\|I - I_0\|_2^2 / N} \right)$$

where N is the number of pixels in the image.

- the SSIM defined as

$$SSIM(I) = \frac{(2\mu_I \mu_{I_0} + c_1)(2cov(I, I_0) + c_2)}{(\mu_I^2 + \mu_{I_0}^2 + c_2)}$$

where μ_x stands for the mean of x , cov is the covariance operator and c_1 and c_2 are constants given for RGB images by $c_1 = (255k_1)^2$ and $c_2 = (255k_2)^2$ with $k_1 = 0.01$ and $k_2 = 0.03$.

9.4 Numerical results for the Gaussian model

An interesting study is the comparison of formula (16a) and (16b) giving the topological gradient for respectively a perforated and a cracked domain. A priori I_{Lap}^b (16a), associated to a perforated domain, would be adapted for the detection of isotropic structures while I_{Lap}^c (16b) would seem more adapted to detect edges straight. Fig. 1 compares, for different values of γ , I_{Lap}^c and I_{Lap}^b to $b(x)$ obtained by minimizing MS (55). For small γ , I_{Lap}^c seems the most robust indicator to detect the black spots contours of the cheetah. We remark by increasing γ that I_{Lap}^b becomes smooth and singular on the entire black spots and not only on its contours, while I_{Lap}^c better detects the border of the cheetah.

We deduce that γ must be tuned with respect to the noise but also by taking into account the size of structures to detect.

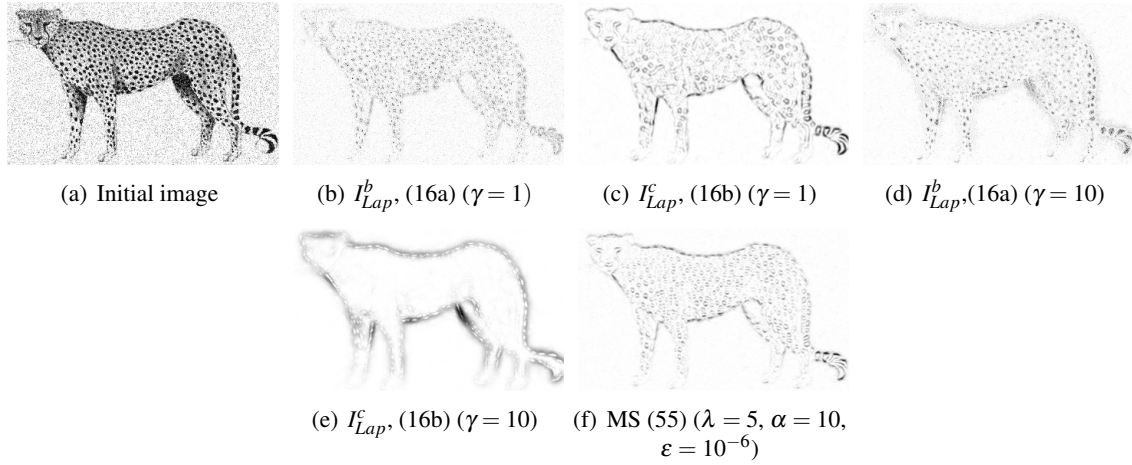


FIGURE 1 – Comparison of the two formula given in (16b) and (16b) for different value of γ with the MS model (55) ($b \approx 0$) for a Gaussian noisy image (PSNR=16dB) containing mainly isotropic small structures.

Fig. 2 shows I_{Lap}^c and the MS result for a Gaussian noisy and Gaussian blurred image. Results are similar but I_{Lap}^c has the advantage of being very fast (for this image the computation time is about one second on a computer equipped with a processor Intel Core 1.9 GHz, see section 9.7 for more details).

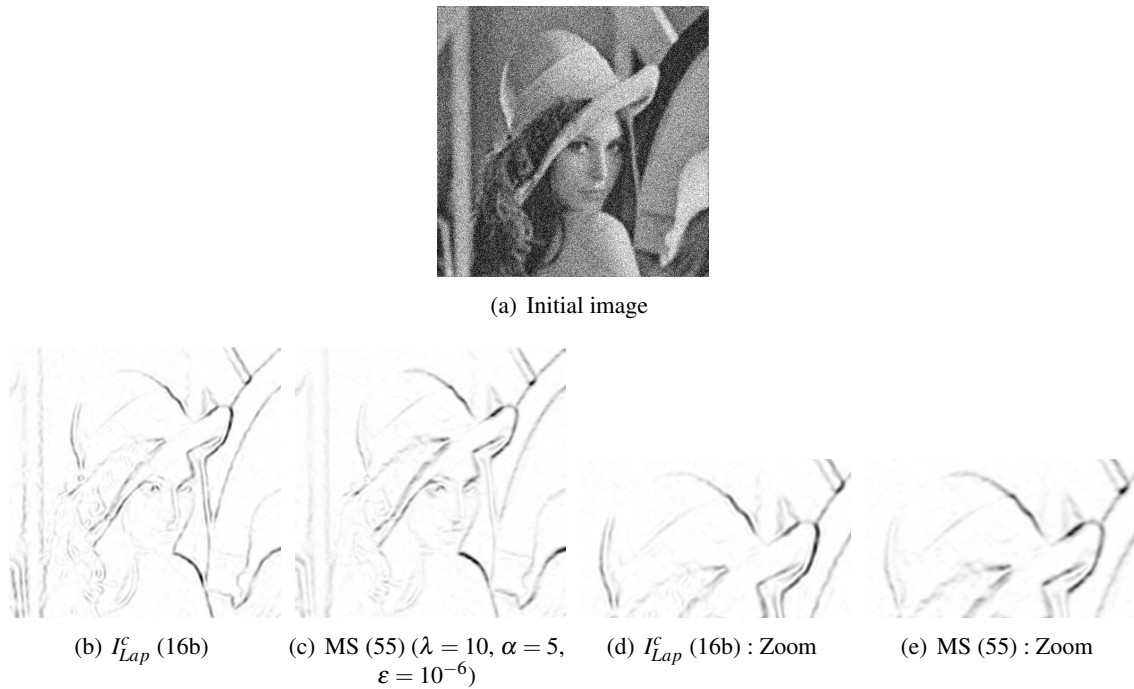


FIGURE 2 – Comparison of the topological gradient (16b) with the MS segmentation (55) on a Gaussian noisy and blurred image (PSNR=16dB, $\sigma = 3$).

Fig. 3 shows the restored version performed by (50), (55) and (56) on a Gaussian noisy and

Gaussian blurred image. We see that the restoration given by MS (55) degrades contours and does not remove completely the blur. Restorations computed by (50) and (56) are quite similar but the computation time is shorter for (50).

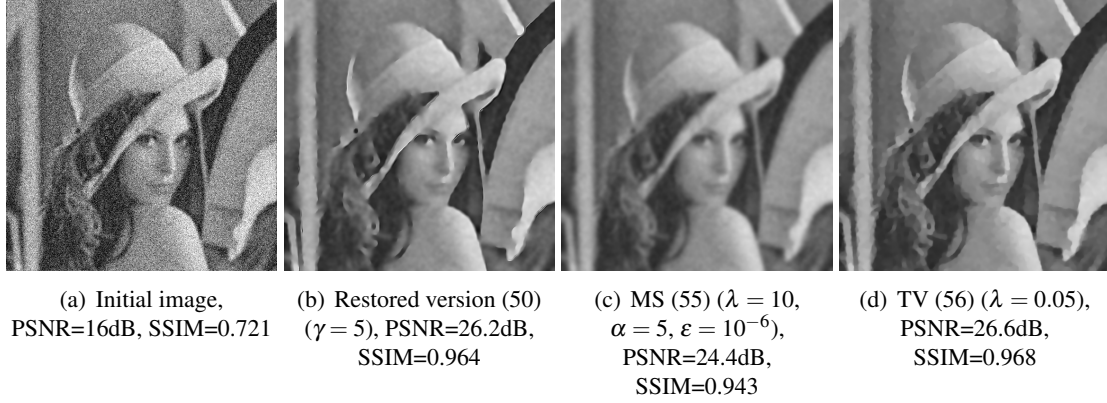


FIGURE 3 – Comparison of restored versions (50), (55) and (56) for a synthetic Gaussian noisy and Gaussian blurred ($\sigma = 3$) image.

Fig. 4 displays the 1D profiles of the image to recover, its degraded versions (blurred, blurred+noisy), the restored version (50) and I_{Lap}^c (16b) across an edge. We see that the restored version matches very well the image to recover and I_{Lap}^c detects quite well the edge.

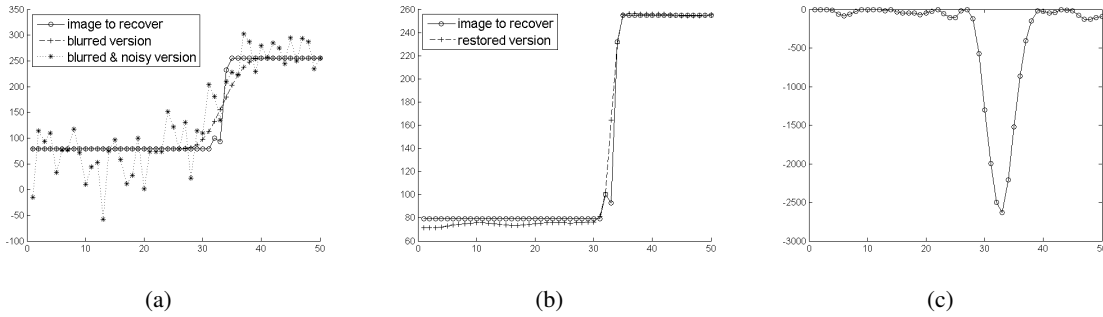


FIGURE 4 – (a) A transverse cut displaying the image to recover, the Gaussian blurred version ($\sigma = 3$), the blurred and noisy version (PSNR=16dB), (b) the restored version (50) ($\gamma = 5$) and (c) the Topological gradient (16b) ($\gamma = 1$).

9.5 Numerical results for the speckle-log model. Comparisons

In this section we still illustrate the segmentation given by I_{Lap}^c (33), I_{Lap}^b (21) and $b(x)$ computed with the MS model (55). We also display the restoration performed by (50), the MS model (55) and the TV model (56).

On Fig. 5, we compare I_{Lap}^c (33) and I_{Lap}^b (21) for different values of γ with the function $b(x)$ given by the MS model for a synthetic speckled image. Similarly to the Gaussian case, I_{Lap}^b seems more adapted to detect isotropic structures and we still deduce that γ must be tuned with respect to

the noise and to the size of structures to detect. Comparing I_{Lap}^c and MS, similar results are obtained for the cheetah.

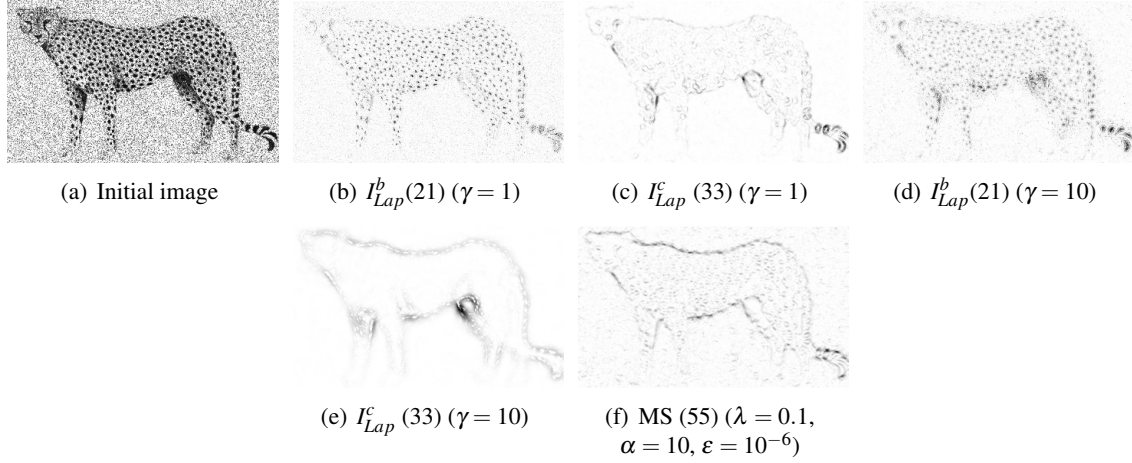


FIGURE 5 – Comparison of the two formula (21) and (33) for different values of γ with the MS segmentation (55) for an initial speckled image ($L = 6$) containing mainly isotropic small structures.

The result given in Fig. 6 for a real SAR image is similar to the one of Fig. 5. Here we see that I_{Lap}^b and I_{Lap}^c can be used for different objectives : particularly on small isotropic structures we see that I_{Lap}^b detects the entire object while I_{Lap}^c detects its edges.

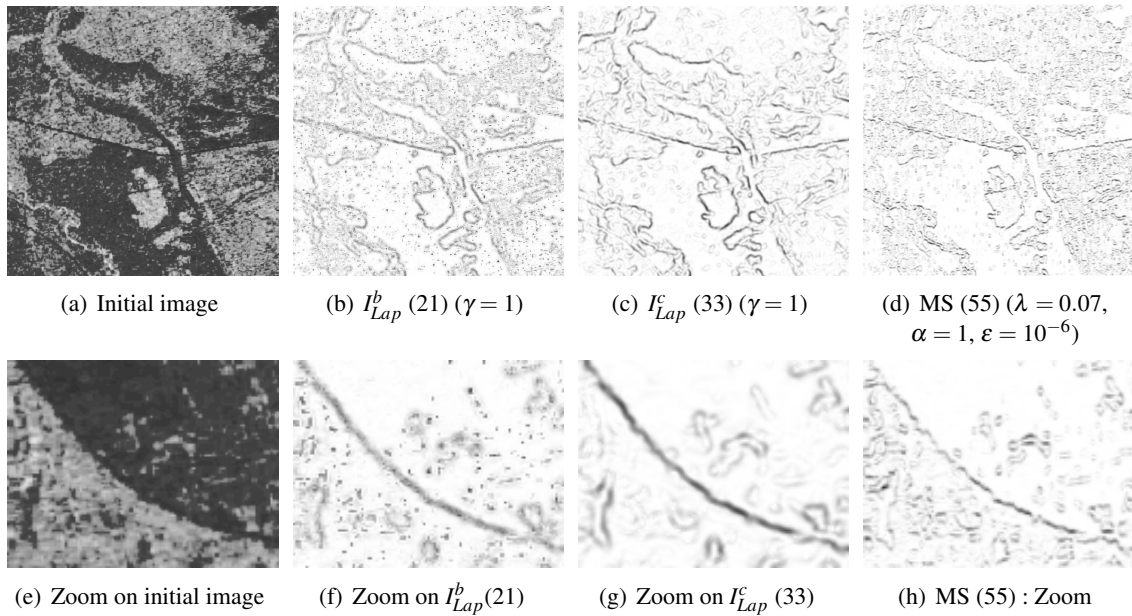


FIGURE 6 – Comparison of the two formula (21) and (33) with the MS segmentation (55) for a real SAR image.

Fig. 7 and Fig. 9 compare the restoration performed by (50), (55) and (56) respectively on a

real SAR image and on a synthetic speckled image. Restoration given by the MS degrades contours while (50) and the TV model (56) are nearly equivalent. However, on Fig. 9, we can notice that the restoration performed by (50) is better than the TV one and computation times are equivalent (see section 9.7).

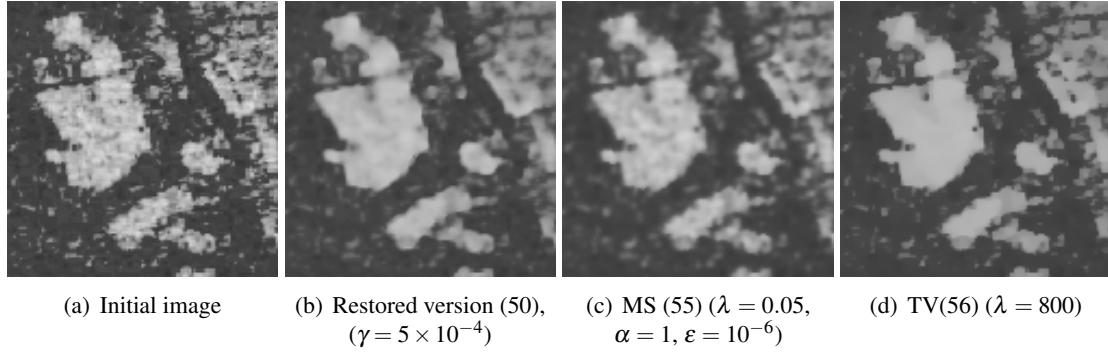


FIGURE 7 – Comparison of restored versions (50), (55) and (56) for a real SAR image (Zoom on Fig. 6-(a)).

On Fig. 8 we compare I_{Lap}^c and $b(x)$ computed with MS (55) for a very noisy synthetic image ($L = 1$ i.e. the worst case for this model). Here I_{Lap}^c gives a quite good result with respect to MS where edges are spread out.

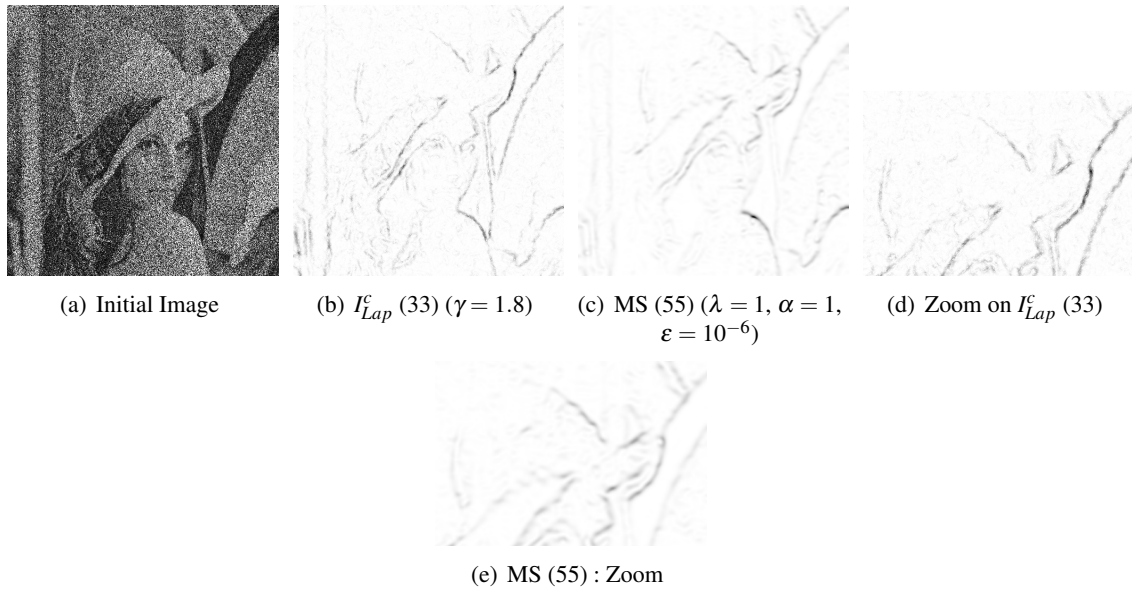


FIGURE 8 – Comparison of the topological gradient (33) with the MS segmentation (55) for a synthetic speckled image ($L = 1$).

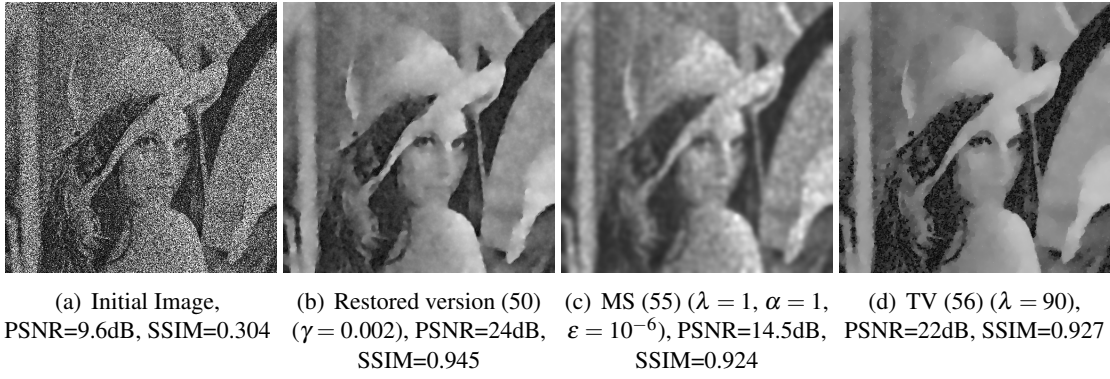


FIGURE 9 – Comparison of restored versions (50), (55) and (56) for a speckled synthetic image ($L = 1$).

Finally Fig. 10 shows the 1D profiles of the image to recover, its noisy version, the restored version (50) and I_{Lap}^c (33) across an edge. The restored version matches very well the image to recover and edges are not degraded. This shows that (50) is a good restoration process.

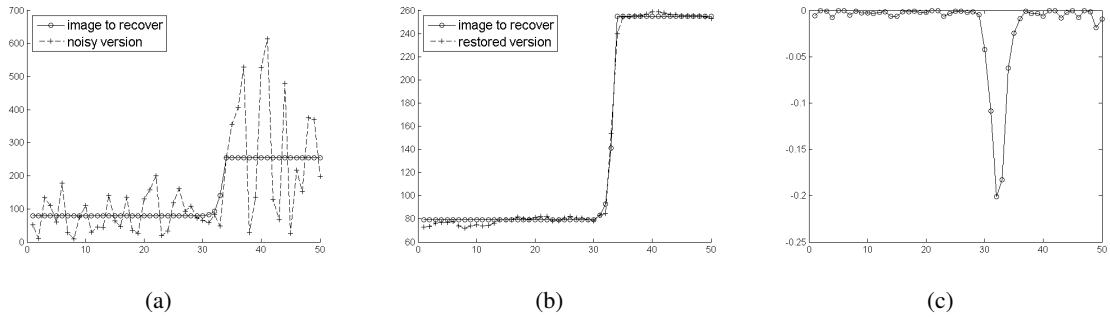


FIGURE 10 – (a) A transverse cut displaying the image to recover and the speckled image, (b) the restored version (50) ($\gamma = 0.002$) and the image to recover, (c) I_{Lap}^c (33) ($\gamma = 1.8$).

9.6 Numerical results for the Poisson model. Comparisons

In this section we compare the segmentation performed by I_{Lap}^c (49), I_{Lap}^b (39) and the MS model (55). We also compare the restoration computed with (50), the MS and the TV model.

Fig. 11 and Fig. 12 show respectively the segmentation results in the case of a synthetic Poissonian image and of a real confocal image of a rat's neuron. I_{Lap}^c (49) detects edges quite well compared to the MS model. We see that I_{Lap}^b fills small structures (the size of these structures is related to γ as for the Gaussian and Poissonian cases).

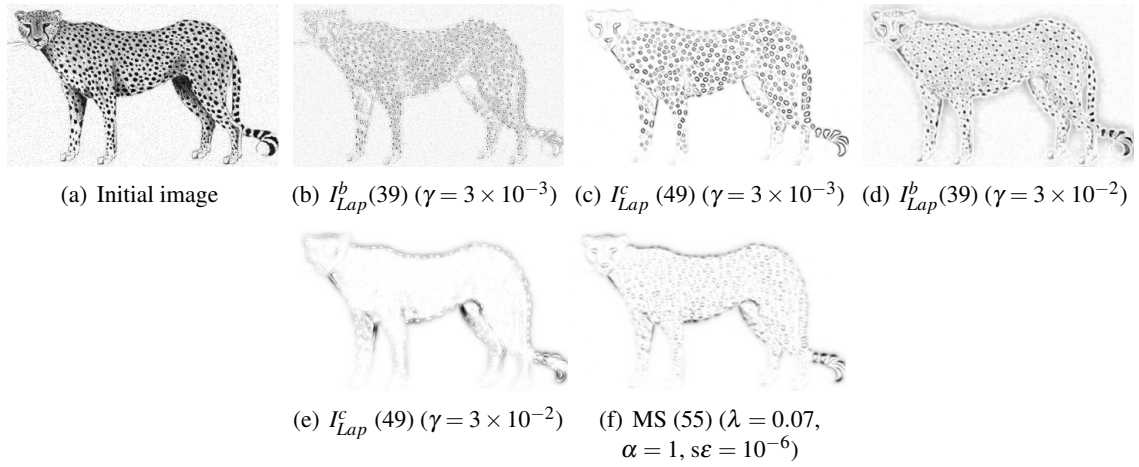


FIGURE 11 – Comparison of the two formula (39) and (49) for different values of γ with the MS segmentation (55) for a Poissonian image containing mainly isotropic small structures.

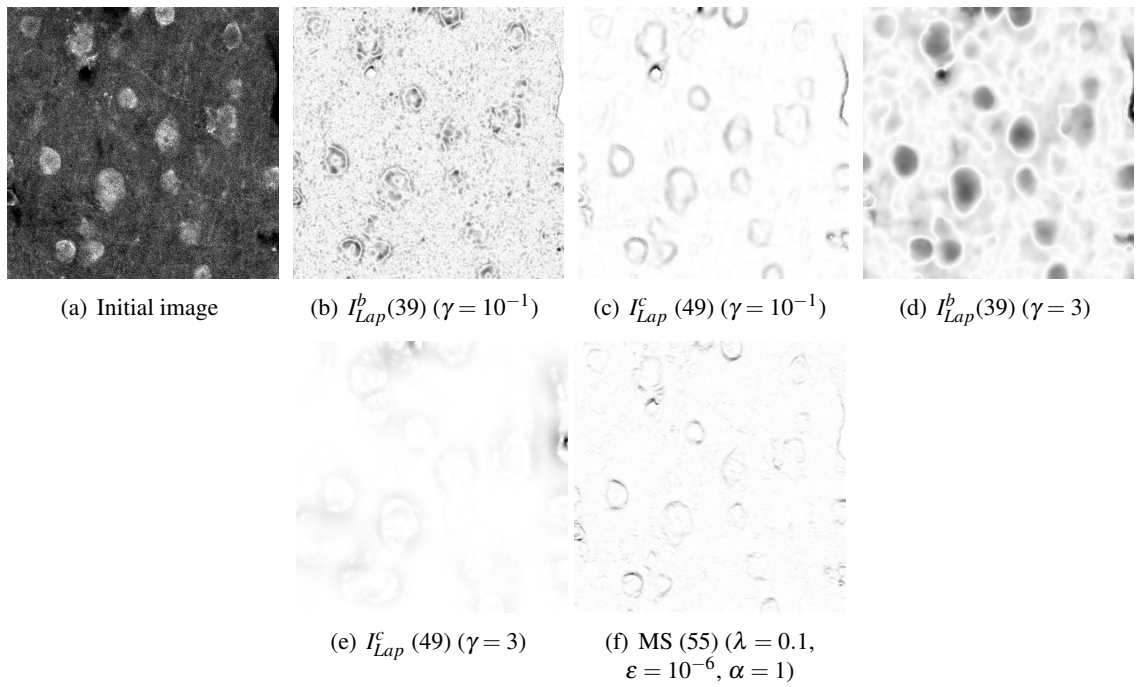


FIGURE 12 – Comparison of the two formula (39) and (49) for different values of γ with the MS segmentation (55) for a Poissonian real image containing rat's neurons.

Fig. 13 and Fig. 15 display the restoration computed by (50), (55) and (56) on respectively a real confocal image and a synthetic Poissonian image blurred by Gaussian convolution. We notice that (50) and (56) restore very well the image preserving edges unlike to the MS model (55) which degrades contours and which does not annihilate the blur effect.

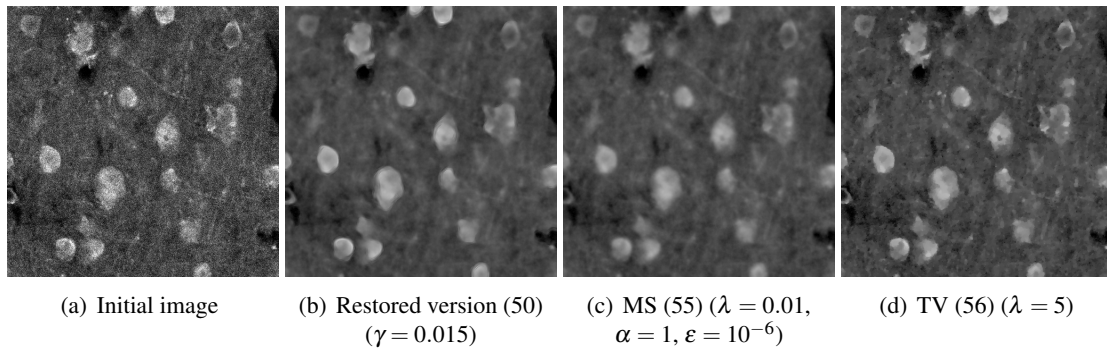


FIGURE 13 – Comparison of the restored versions (50), (55) and (56) for a real Poissonian image of rat's neurons.

Fig. 14 compares I_{Lap}^c (49) with $b(x)$ performed by the MS model (55) for a Poissonian image blurred by a Gaussian convolution.

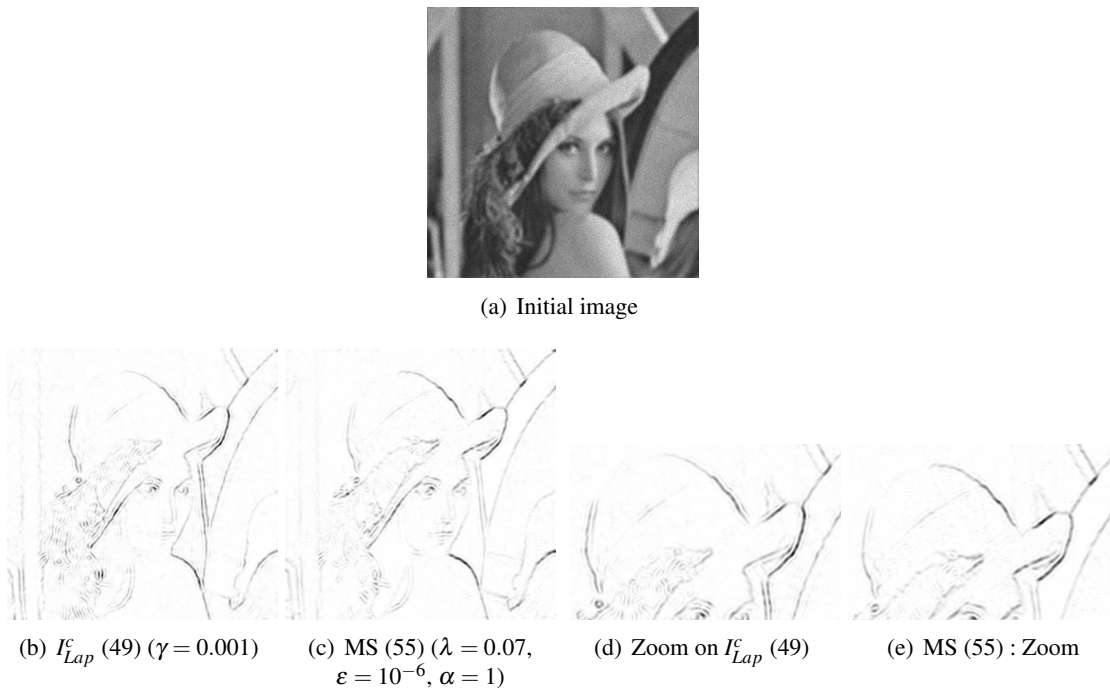


FIGURE 14 – Comparison of I_{Lap}^c (49) with the MS segmentation (55) on a synthetic Poissonian image.

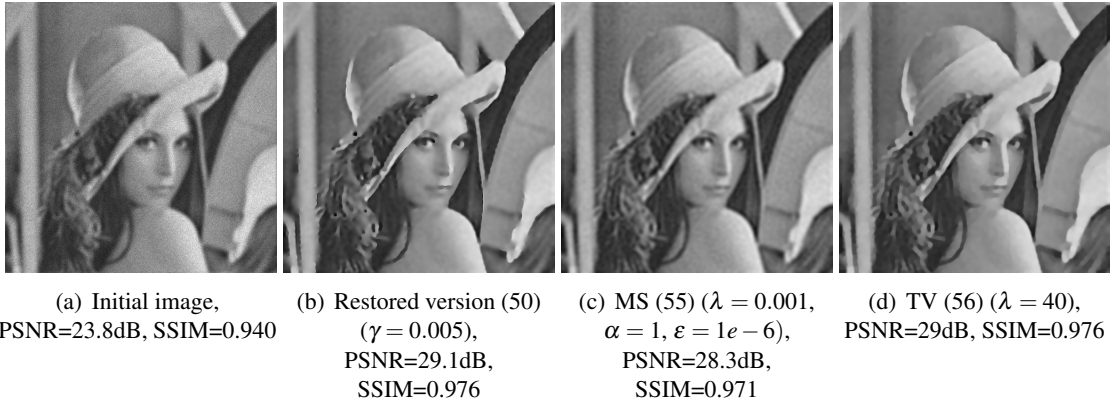


FIGURE 15 – Comparison of the restored versions for a Poissonian image blurred by Gaussian convolution ($\sigma = 3$).

Finally, Fig. 16 shows the 1D profiles of the image to recover, its degraded versions (blurred, blurred + Poissonian process), the restored version (50) and I_{Lap}^c (49) across an edge. We see that (50) allows to recover the initial image and that I_{Lap}^c detects very well the edge.

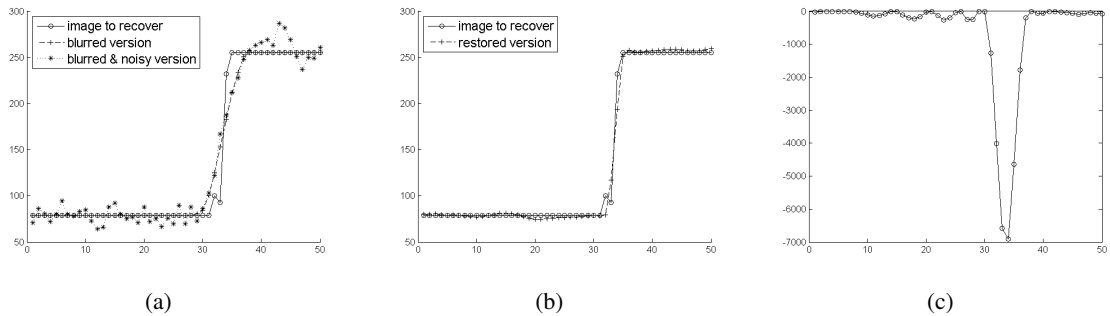


FIGURE 16 – (a) A transverse cut displaying the image to recover, the Gaussian blurred version ($\sigma = 3$), the blurred and noisy version (PSNR=16dB), (b) the restored version (50) ($\gamma = 0.005$) and (c) I_{Lap}^c (16b) ($\gamma = 0.001$).

9.7 Computational time comparisons for the three methods

On Fig. 17 and Fig. 18 are compared the three methods for $K = I$ (no blur) : Mumford-Shah (MS), TV and the topological gradient method (TG). The experiments are performed on a computer equipped with a processor Intel Core 1.9 GHz and all algorithms are implemented in Matlab. In the Gaussian case, since all the equations are linear, the topological gradient method is the fastest method both for segmentation and restoration. To fix ideas, for an image containing 6.4×10^5 pixels, the computational time for the segmentation performed by the topological gradient is less than one second and the restoration is about four seconds.

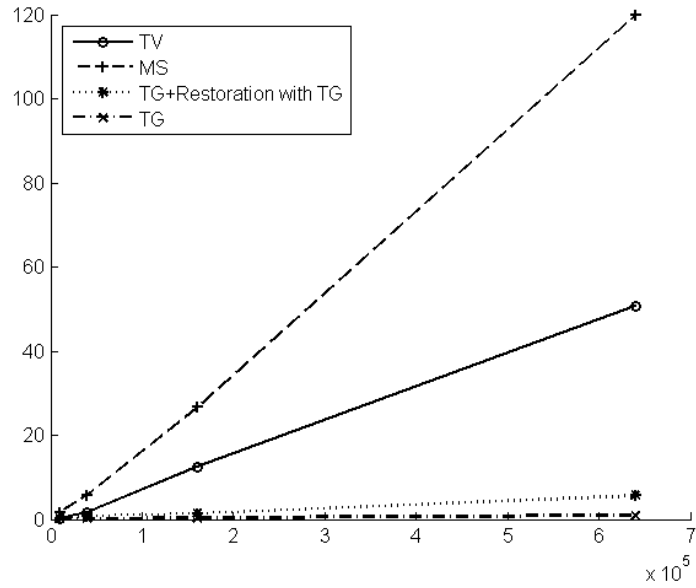


FIGURE 17 – Comparisons of the computational time of the three methods in function of the number of pixels in the Gaussian case

For the nonlinear cases (Poissonian and speckle models), the computation of the topological gradient still remains the fastest but the restoration step performed by (50) takes approximately the same time as for a restoration given by a TV model. Let us notice that the TV model is implemented by using an iterative algorithm (explicit schema with fixed step length with at maximum 1000 iterations) and that the Mumford-Shah model solution is computed by minimizing the approximate functional alternatively with respect to u and b . When this latter model is associated to non quadratic data fidelity terms (Poisson and speckle), the minimization with respect to u (at b fixed) is made by using Algorithm 3 and we perform 15 iterations. Finally let us precise that we present on Fig. 18 the computation time only for the Poissonian model because similar results are obtained from the speckle one.

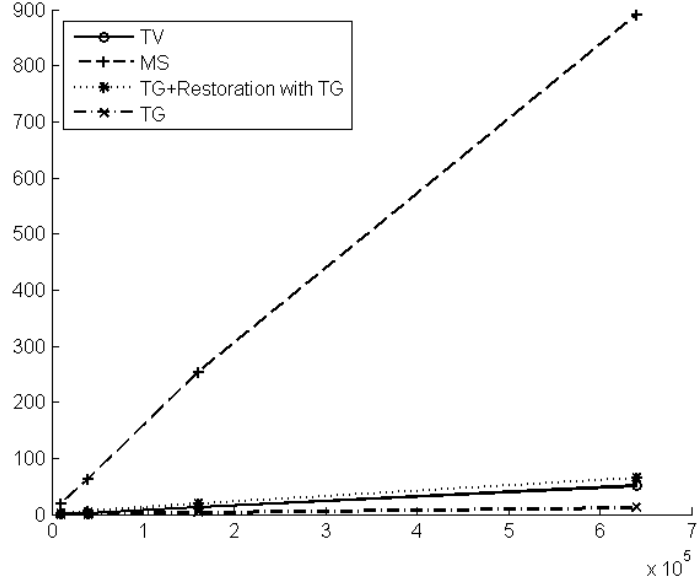


FIGURE 18 – Comparisons of the computational time of the three methods of restoration in function of the number of pixels in the Poissonian case

10 Appendices

In these appendices we give the asymptotic expansion of the differences $u_\varepsilon - u_0$ and $v_\varepsilon - v_0$ for the non linear problems (Poisson and Speckle-log models). Some proofs are similar to the linear case and so we will refer the reader to [4]. To establish these asymptotic expansions we need the following exterior problem

$$(\mathcal{P}_{ext}) \begin{cases} \Delta H = 0, \text{ on } \mathbb{R}^2 \setminus \bar{B} \\ \partial_n H = g, \text{ on } \partial B \\ H \longrightarrow 0, \text{ at } \infty \end{cases} \quad (57)$$

where $g \in H^{-1/2}(\partial B)$ and $\int_{\partial B} g d\sigma = 0$. For the computation of the topological gradient we will use the two following lemma. We omit the proofs and we refer the reader to [21] for more details

Lemma 10.1. *The solution of (57) expresses as a simple layer potential :*

$$H(x) = \int_{\partial B} \lambda(y) E(x-y) d\sigma$$

with $E(x) = -\frac{1}{2\pi} \log(|x|)$ is the fundamental solution of the Laplace operator and $\lambda(y) = -2g(y)$. Denoting by l^H the solution of (29), we have the jump relations through ∂B

$$\begin{aligned} H - l^H &= 0 \\ \partial_n H - \partial_n l^H &= -\lambda \end{aligned}$$

and l^u expresses also as $l^H(x) = \int_{\partial B} \lambda(y) E(x-y) d\sigma$.

The following asymptotic estimations holds.

Lemma 10.2. *Let H the solution of (57), then :*

$$\begin{aligned} |H(x)| &\leq \frac{C}{|x|}, & |\nabla H(x)| &\leq \frac{C}{|x|^2} \\ \left\| H\left(\frac{x}{\varepsilon}\right) \right\|_{0, \Omega_\varepsilon} &= O\left(\sqrt{-\log(\varepsilon)}\right), & \left\| \nabla H\left(\frac{x}{\varepsilon}\right) \right\|_{0, \Omega_\varepsilon} &= O(\varepsilon) \end{aligned}$$

10.1 Appendix A

In this appendix all the proofs are performed assuming $\gamma = 1$, and when (19) is referenced we suppose that $\gamma = 1$. Moreover we suppose that ψ fulfills Hypotheses 1.

Lemma 10.3. *Let $X_\varepsilon = u_\varepsilon - u_0$ where u_ε and u_0 are respectively given by (19) for $\varepsilon > 0$ and $\varepsilon = 0$, and let P be the solution of (57) with $g = -\nabla u_0(0) \cdot n$, then we have the following asymptotic expansion :*

$$X_\varepsilon = \varepsilon P\left(\frac{x}{\varepsilon}\right) + e_\varepsilon$$

with $\|e_\varepsilon\|_{1, \Omega_\varepsilon} = O(\varepsilon^2 \sqrt{-\log(\varepsilon)})$. Moreover we have the following estimation

$$\|X_\varepsilon\|_{0, \Omega_\varepsilon} = O\left(\varepsilon^2 \sqrt{-\log(\varepsilon)}\right)$$

Démonstration. First by subtracting equations (19) for $\varepsilon > 0$ and $\varepsilon = 0$:

$$\begin{cases} -\Delta X_\varepsilon + D_u \psi(x, u_\varepsilon) - D_u \psi(x, u_0) = 0, & \text{on } \Omega_\varepsilon \\ \partial_n X_\varepsilon = -\partial_n u_0, & \text{on } \partial B_\varepsilon \\ \partial_n X_\varepsilon = 0, & \text{on } \Gamma \end{cases} \quad (58)$$

Then an integration by parts gives :

$$\int_{\Omega_\varepsilon} \nabla X_\varepsilon \cdot \nabla v + \int_{\Omega_\varepsilon} (D_u \psi(x, u_\varepsilon) - D_u \psi(x, u_0)) v = - \int_{\partial B_\varepsilon} \nabla u_0(0) \cdot \vec{n} v \quad \forall v \in H^1(\Omega_\varepsilon) \quad (59)$$

With a similar manner we integrate by parts the Euler equation checked by $\varepsilon P\left(\frac{x}{\varepsilon}\right)$ on Ω_ε :

$$\int_{\Omega_\varepsilon} \nabla P\left(\frac{x}{\varepsilon}\right) \cdot \nabla v = - \int_{\partial B_\varepsilon} \nabla u_0(0) \cdot \vec{n} - \int_\Gamma \partial_n P\left(\frac{x}{\varepsilon}\right) v \quad (60)$$

By setting $e_\varepsilon = X_\varepsilon - \varepsilon P\left(\frac{x}{\varepsilon}\right)$ and subtracting (59) to (60), we get

$$\int_{\Omega_\varepsilon} \nabla e_\varepsilon \cdot \nabla v + \int_{\Omega_\varepsilon} (D_u \psi(x, u_\varepsilon) - D_u \psi(x, u_0)) v = - \int_\Gamma \partial_n P\left(\frac{x}{\varepsilon}\right) v - \int_{\partial B_\varepsilon} (\partial_n u_0 - \nabla u_0(0) \cdot \vec{n}) v$$

Then, thanks to a Taylor expansion, we rewrite the second term on the right hand-side of the above equality : $D_u \psi(x, u_\varepsilon) - D_u \psi(x, u_0) = D_u^2 \psi(x, u_{\delta_\varepsilon})(u_\varepsilon - u_0)$ with $u_{\delta_\varepsilon} = \theta u_0 + (1 - \theta) u_\varepsilon$, $\theta : \Omega \rightarrow \mathbb{R}$, $0 \leq \theta \leq 1$. We can bound from below this term by using Lemma 5.1 and Hypotheses 1. Indeed, since $a \leq u_{\delta_\varepsilon} \leq b$ and $\psi(u)$ is strictly convex on $[a, b] \subset I$, we get that there exists $\delta > 0$ not depending on ε such that $D_u^2 \psi(x, u_{\delta_\varepsilon}) \geq \delta > 0$. Thus e_ε is solution of the following well-posed variational problem : find $e_\varepsilon \in H^1(\Omega_\varepsilon)$ such that

$$\begin{aligned} \int_{\Omega_\varepsilon} \nabla e_\varepsilon \cdot \nabla v + \int_{\Omega_\varepsilon} D_u^2 \psi(x, u_{\delta_\varepsilon}) e_\varepsilon v &= - \int_\Gamma \partial_n P\left(\frac{x}{\varepsilon}\right) v - \int_{\partial B_\varepsilon} (\partial_n u_0 - \nabla u_0(0) \cdot \vec{n}) v \\ &\quad - \int_{\Omega_\varepsilon} D_u^2 \psi(x, u_{\delta_\varepsilon}) \varepsilon P\left(\frac{x}{\varepsilon}\right) v \end{aligned}$$

for all $v \in H^1(\Omega_\varepsilon)$. Now we split e_ε in $e_\varepsilon = e_\varepsilon^1 + e_\varepsilon^2$ with

(i) $e_\varepsilon^1 \in H^1(\Omega_\varepsilon)/\mathbb{R}$ solution of

$$\int_{\Omega_\varepsilon} \nabla e_\varepsilon^1 \cdot \nabla v = - \int_{\partial B_\varepsilon} (\partial_n u_0 - \nabla u_0(0) \cdot \vec{n}) v \quad \forall v \in H^1(\Omega_\varepsilon)$$

(ii) $e_\varepsilon^2 \in H^1(\Omega_\varepsilon)$ solution of

$$\int_{\Omega_\varepsilon} \nabla e_\varepsilon^2 \cdot \nabla v + \int_{\Omega_\varepsilon} D_u^2 \psi(x, u_{\delta_\varepsilon}) e_\varepsilon^2 v = - \int_\Gamma \partial_n P \left(\frac{x}{\varepsilon} \right) v - \int_{\Omega_\varepsilon} D_u^2 \psi(x, u_{\delta_\varepsilon}) \left(\varepsilon P \left(\frac{x}{\varepsilon} \right) + e_\varepsilon^1 \right)$$

Then, by using a change of variable (CV), a trace theorem on $B_2 \setminus \bar{B}$ (where B_2 is the ball of radius 2, centered at 0), and the equivalency of the $H^1(B_2 \setminus \bar{B})$ -norm with the semi-norm and a CV again, we get that $\|e_\varepsilon\|_{H^1(\Omega_\varepsilon)/\mathbb{R}} = O(\varepsilon^2)$. Next, by using Lemma 10.2, a trace Theorem on $\Omega \setminus \bar{B}$ and the fact that $e_\varepsilon^1 \in H^1(\Omega_\varepsilon)/\mathbb{R}$, we get that $\|e_\varepsilon^2\|_{1, \Omega_\varepsilon} = O(\varepsilon^2 \sqrt{-\log(\varepsilon)})$. The $H^1(\Omega_\varepsilon)$ -norm estimation of e_ε is then straightforward by using these two estimations and the following inequality $\|e_\varepsilon\|_{1, \Omega_\varepsilon} \leq \|e_\varepsilon^1\|_{H^1(\Omega_\varepsilon)/\mathbb{R}} + \|e_\varepsilon^2\|_{1, \Omega_\varepsilon}$; the estimation of $\|X_\varepsilon\|_{0, \Omega_\varepsilon}$ comes from $\|X_\varepsilon\|_{0, \Omega_\varepsilon} \leq \|\varepsilon P \left(\frac{x}{\varepsilon} \right)\|_{0, \Omega_\varepsilon} + \|e_\varepsilon\|_{0, \Omega_\varepsilon}$ and the previous inequalities. This ends the proof. For more details we refer the reader to [21]. \square

Lemma 10.4. *Let $w_\varepsilon = v_\varepsilon - v_0$ where v_ε and v_0 are respectively given by (25) for $\varepsilon > 0$ and $\varepsilon = 0$, and let Q be the the solution of (57) with $g = -\nabla v_0(0) \cdot n$, then we have the following asymptotic expansion :*

$$w_\varepsilon = \varepsilon Q \left(\frac{x}{\varepsilon} \right) + r_\varepsilon$$

with $\|r_\varepsilon\|_{1, \Omega_\varepsilon} = O(\varepsilon^2 \sqrt{-\log(\varepsilon)})$. Moreover we have

$$\|w_\varepsilon\|_{0, \Omega_\varepsilon} = O \left(\varepsilon^2 \sqrt{-\log(\varepsilon)} \right) \quad , \quad |w_\varepsilon|_{1, \Omega_\varepsilon} = O(\varepsilon)$$

Démonstration. The problem is linear. From Lemma 5.1 and Hypotheses 1, we get that there exist $\delta_1 > 0$ and $\delta_2 > 0$ such that $\delta_2 \geq D_u^2 \psi(u_0) \geq \delta_1$. The well-posedness of the problem is then straightforward. Then the proof can be easily deduced from the proof of Theorem 10.3 or from the linear case [4]. \square

10.2 Appendix B

In this appendix we consider problem (38) with $K = I$ and $\gamma = 1$. The general case (when K is a convolution operator such that $K\mathbb{1} \neq 0$) can be easily deduced (see [7] chapter 3 for the well-posedness).

Lemma 10.5. *Let $X_\varepsilon = u_\varepsilon - u_0$ where u_ε and u_0 are respectively given by (38) for $\varepsilon > 0$ and $\varepsilon = 0$, then we have :*

$$X_\varepsilon = \varepsilon P \left(\frac{x}{\varepsilon} \right) + e_\varepsilon$$

where P is defined by (57) with $g = -\nabla u_0(0) \cdot \vec{n}$ and where $\|e_\varepsilon\|_{1, \Omega_\varepsilon} = O(\varepsilon^2)$. Moreover we have the estimation :

$$\|X_\varepsilon\|_{0, \Omega_\varepsilon} = O(\varepsilon^2 \sqrt{-\log(\varepsilon)})$$

Démonstration. First, let us write the Euler equations checked by X_ε . By subtracting equations (38) for $\varepsilon > 0$ and for $\varepsilon = 0$, we get for $j \in I_{ind}(\Omega)$:

$$(\mathcal{X}_\varepsilon) \left\{ \begin{array}{l} -\Delta X_\varepsilon + D\psi_j \left(\int_{R_j^\varepsilon} u_\varepsilon \right) - D\psi_j \left(\int_{R_j} u_0 \right) = 0 \\ \text{on } R_j^\varepsilon, j \in I_{ind}(\Omega) \\ \partial_n X_\varepsilon = -\partial_n u_0, \text{ on } \partial B_\varepsilon \\ \partial_n X_\varepsilon = 0, \text{ on } \Gamma \end{array} \right. \quad (61)$$

Then, by a Taylor expansion there exists $\xi_\varepsilon = \theta \int_{R_j^\varepsilon} u_\varepsilon + (1 - \theta) \int_{R_j} u_0$ with $0 < \theta < 1$ such that

$$D\psi_j \left(\int_{R_j^\varepsilon} u_\varepsilon \right) - D\psi_j \left(\int_{R_j} u_0 \right) = D^2\psi_j(\xi_\varepsilon) \left(\int_{R_j^\varepsilon} u_\varepsilon - \int_{R_j} u_0 \right)$$

From Proposition 3, it is straightforward that $0 < \alpha \leq \xi_\varepsilon \leq \beta$ where $\alpha = \frac{\min_i f_i}{N}$ and $\beta = \sum_i f_i$. $(\mathcal{X}_\varepsilon)$ rewrites for $j \in I_{ind}(\Omega)$ as

$$(\mathcal{X}_\varepsilon) \left\{ \begin{array}{l} -\Delta X_\varepsilon + D^2\psi_j(\xi_\varepsilon) \int_{R_j^\varepsilon} X_\varepsilon = \int_{R_j \setminus \overline{R_j^\varepsilon}} u_0 \text{ on } R_j^\varepsilon \\ \partial_n X_\varepsilon = -\partial_n u_0, \text{ on } \partial B_\varepsilon \\ \partial_n X_\varepsilon = 0, \text{ on } \Gamma \end{array} \right.$$

with $\int_{R_j \setminus \overline{R_j^\varepsilon}} u_0 = \delta_{j_0}(j) \int_{B_\varepsilon} u_0$, where δ is the Dirac function. Let $e_\varepsilon = X_\varepsilon - \varepsilon P\left(\frac{x}{\varepsilon}\right)$ where P is defined by (57) with $g = -\nabla u_0(0) \cdot \vec{n}$. e_ε , then e_ε verifies the following equation

$$(\mathcal{E}_\varepsilon) \left\{ \begin{array}{l} -\Delta e_\varepsilon + D^2\psi_j(\xi_\varepsilon) \int_{R_j^\varepsilon} e_\varepsilon = -\varepsilon D^2\psi_j(\xi_\varepsilon) \int_{R_j^\varepsilon} P\left(\frac{x}{\varepsilon}\right) \\ \text{on } R_j^\varepsilon, j \in I_{ind}(\Omega) \\ \partial_n e_\varepsilon = -(\partial_n u_0 - \nabla u_0(0) \cdot \vec{n}) = \varphi_\varepsilon(x) = O(|x|) \text{ on } \partial B_\varepsilon \\ \partial_n e_\varepsilon = -\partial_n P\left(\frac{x}{\varepsilon}\right) = \phi_\varepsilon(x) = O\left(\frac{\varepsilon^2}{|x|^2}\right) \text{ on } \Gamma \end{array} \right. \quad (62)$$

We set :

$$K_\varepsilon^j = \left\{ \begin{array}{l} -\varepsilon D^2\psi_j(\xi_\varepsilon) \int_{R_j} P\left(\frac{x}{\varepsilon}\right) = O(\varepsilon^3), \text{ for } j \neq j_0 \\ \int_{B_\varepsilon} u_0 - \varepsilon D^2\psi_{j_0}(\xi_\varepsilon) \int_{R_{j_0}^\varepsilon} P\left(\frac{x}{\varepsilon}\right) = O(\varepsilon^2), \text{ for } j = j_0 \end{array} \right.$$

Now we split e_ε in the sum $e_\varepsilon = e_\varepsilon^1 + e_\varepsilon^2 + e_\varepsilon^3$ with

(i) $e_\varepsilon^1 \in H^1(\Omega_\varepsilon)/\mathbb{R}$ solution of

$$\left\{ \begin{array}{l} -\Delta e_\varepsilon^1 = 0, \text{ on } \Omega_\varepsilon \\ \partial_n e_\varepsilon^1 = \varphi_\varepsilon(x), \text{ on } \partial B_\varepsilon \\ \partial_n e_\varepsilon^1 = 0, \text{ on } \Gamma \end{array} \right.$$

(ii) $e_\varepsilon^2 \in H^1(\Omega_\varepsilon)/\mathbb{R}$ solution of

$$\left\{ \begin{array}{l} \Delta e_\varepsilon^2 = 0, \text{ on } \Omega_\varepsilon \\ \partial_n e_\varepsilon^2 = 0, \text{ on } \partial B_\varepsilon \\ \partial_n e_\varepsilon^2 = \phi_\varepsilon(x), \text{ on } \Gamma \end{array} \right.$$

(iii) $e_\varepsilon^3 \in H^1(\Omega_\varepsilon)$ solution of

$$(\mathcal{E}_\varepsilon^3) \left\{ \begin{array}{l} -\Delta e_\varepsilon^3 + D^2 \psi_j(\xi_\varepsilon) \int_{R_j} e_\varepsilon^3 = K_\varepsilon^j - D^2 \psi_j(\xi_\varepsilon) \int_{R_j^\varepsilon} (e_\varepsilon^2 + e_\varepsilon^2) \\ \text{on } R_j^\varepsilon, j \in I_{ind}(\Omega) \\ \partial_n e_\varepsilon^3 = 0, \text{ on } \partial B_\varepsilon \\ \partial_n e_\varepsilon^3 = 0, \text{ on } \Gamma \end{array} \right.$$

Standard computations (see [4, 21] for more details) lead to the following estimations :

$$\|e_\varepsilon^1\|_{H^1(\Omega_\varepsilon)/\mathbb{R}} \leq C\varepsilon^2 \quad \|e_\varepsilon^2\|_{H^1(\Omega_\varepsilon)/\mathbb{R}} \leq C\varepsilon^2$$

To estimate e_ε^3 , we take the variational formulation of $(\mathcal{E}_\varepsilon^3)$:

$$\int_{\Omega_\varepsilon} \nabla e_\varepsilon^3 \cdot \nabla v + \sum_{j \in I_{ind}(\Omega)} D^2 \psi_j(\xi_\varepsilon) \int_{R_j^\varepsilon} e_\varepsilon^3 \int_{R_j^\varepsilon} v = \sum_{j \in I_{ind}(\Omega)} K_\varepsilon^j \int_{R_j^\varepsilon} v - D^2 \psi_j^\varepsilon(\xi_\varepsilon) \int_{R_j^\varepsilon} (e_\varepsilon^1 + e_\varepsilon^2) \int_{R_j^\varepsilon} v \quad (63)$$

An easy computation of $D^2 \psi_j$ and Proposition 3 give for $\varepsilon \leq \varepsilon_0$

$$\frac{\max_{j \in I_{ind}(\Omega)} f_j}{\alpha^2} \geq D^2 \psi_j(\xi_\varepsilon) = \frac{f_j}{\xi_\varepsilon^2} \geq \frac{\min_{j \in I_{ind}(\Omega)} f_j}{\beta^2} > 0$$

where $N = |I_{ind}(\Omega)|$. By taking as test function $v = e_\varepsilon^3$ in (63), we deduce the following estimations :

$$\begin{aligned} & \int_{\Omega_\varepsilon} |\nabla e_\varepsilon^3|^2 + C \sum_{j \in I_{ind}(\Omega)} \left(\int_{R_j^\varepsilon} e_\varepsilon^3 \right)^2 \\ & \leq \sum_{j \in I_{ind}(\Omega)} |K_\varepsilon^j| \left| \int_{R_j^\varepsilon} e_\varepsilon^3 \right| + |D^2 \psi_j^\varepsilon(\xi_\varepsilon)| \int_{R_j^\varepsilon} (|e_\varepsilon^1| + |e_\varepsilon^2|) \left| \int_{R_j^\varepsilon} e_\varepsilon^3 \right| \\ & \leq C \left(\varepsilon^2 + \|e_\varepsilon^1\|_{L^2(\Omega_\varepsilon)/\mathbb{R}} + \|e_\varepsilon^2\|_{L^2(\Omega_\varepsilon)/\mathbb{R}} \right) \sum_{j \in I_{ind}(\Omega)} \left| \int_{R_j^\varepsilon} e_\varepsilon^3 \right| \\ & \leq C\varepsilon^2 \sum_{j \in I_{ind}(\Omega)} \left| \int_{R_j^\varepsilon} e_\varepsilon^3 \right| \end{aligned}$$

Then, thanks to the following inequality which stands for any sequence of real numbers $(a_i)_i$

$$\left(\sum_{i \in I_{ind}(\Omega)} |a_i| \right)^2 \leq |I_{ind}(\Omega)| \sum_{i \in I_{ind}(\Omega)} |a_i|^2$$

and the positiveness of $\int_{\Omega_\varepsilon} |\nabla e_\varepsilon^3|^2$, we obtain

$$\sum_{j \in I_{ind}(\Omega)} \left| \int_{R_j^\varepsilon} e_\varepsilon^3 \right| \leq C\varepsilon^2$$

and then $|e_\varepsilon^3|_{1, \Omega_\varepsilon} \leq C\varepsilon^2$. By using the Poincaré-Wirtinger inequality we get :

$$\begin{aligned} \|e_\varepsilon^3\|_{1, \Omega_\varepsilon} & \leq \left\| e_\varepsilon^3 - \frac{1}{|\Omega|} \int_{\Omega_\varepsilon} e_\varepsilon^3 \right\|_{1, \Omega_\varepsilon} + \left| \int_{\Omega_\varepsilon} e_\varepsilon^3 \right| \\ & \leq C|e_\varepsilon^3|_{1, \Omega_\varepsilon} + C \sum_{j \in I_{ind}(\Omega)} \left| \int_{R_j^\varepsilon} e_\varepsilon^3 \right| \leq C\varepsilon^2 \end{aligned}$$

From the inequality $\|e_\varepsilon\|_{1,\Omega_\varepsilon} \leq \|e_\varepsilon^1\|_{H^1(\Omega_\varepsilon)/\mathbb{R}} + \|e_\varepsilon^2\|_{H^1(\Omega_\varepsilon)/\mathbb{R}} + \|e_\varepsilon^3\|_{1,\Omega_\varepsilon}$, we get the result. For the $L^2(\Omega_\varepsilon)$ -norm estimation of X_ε , it suffices to take the $L^2(\Omega_\varepsilon)$ -norm of its asymptotic expansion and to use the first point of Lemma 10.5 and Lemma 10.2. \square

Lemma 10.6. *Let $w_\varepsilon = v_\varepsilon - v_0$ where v_ε and v_0 are given by (43) for $\varepsilon > 0$ and $\varepsilon = 0$, then we have :*

$$w_\varepsilon = \varepsilon Q\left(\frac{x}{\varepsilon}\right) + r_\varepsilon$$

where Q is defined by (57) with $g = -\nabla v_0(0) \cdot n$, and where $\|r_\varepsilon\|_{1,\Omega_\varepsilon} = O(\varepsilon^2 \sqrt{-\log(\varepsilon)})$. Moreover we have :

$$\|w_\varepsilon\|_{0,\Omega_\varepsilon} = O(\varepsilon^2 \sqrt{-\log(\varepsilon)}), \quad |w_\varepsilon|_{1,\Omega_\varepsilon} = O(\varepsilon)$$

Démonstration. By subtracting equations (44) for $\varepsilon > 0$ and for $\varepsilon = 0$, the Euler equations associated to w_ε are :

$$(\mathcal{W}_\varepsilon) \left\{ \begin{array}{l} -\Delta w_\varepsilon + D^2 \psi_j(I_j(u_0)) \int_{R_j^\varepsilon} w_\varepsilon = 0 \text{ on } R_j \text{ with } j \neq j_0 \\ -\Delta w_\varepsilon + D^2 \psi_{j_0}(I_{j_0}(u_0)) \int_{R_{j_0}^\varepsilon} w_\varepsilon \\ = D^2 \psi_{j_0}(I_{j_0}(u_0)) \int_{B_\varepsilon} v_0 = O(\varepsilon^2) \text{ on } R_{j_0}^\varepsilon \\ \partial_n w_\varepsilon = -\partial_n v_0 \text{ on } \partial B_\varepsilon \\ \partial_n w_\varepsilon = 0 \text{ on } \Gamma \end{array} \right. \quad (64)$$

This problem is linear and from (3) we have :

$$\frac{\max_{j \in I_{\text{ind}}(\Omega)} f_j}{\alpha^2} \geq D^2 \psi_j(I_j(u_0)) = \frac{f_j}{I_j(u_0)^2} \geq \frac{\min_{j \in I_{\text{ind}}(\Omega)} f_j}{\beta^2}$$

Then the topological expansion of w_ε can be deduced from the proof of Lemma 10.5 or from the linear case [4].

The two last estimations are straightforward by using the topological expansion of w_ε and Lemma 10.2. \square

Références

- [1] L. Ambrosio and V.M. Tortorelli. Approximation of functionals depending on jumps by elliptic functionals via Gamma-convergence. *Communications on Pure and Applied Mathematics*, XLIII :999–1036, 1990.
- [2] S. Amstutz. Topological sensitivity analysis for some nonlinear PDE system. *J. Math. Pures Appl.*, 2006.
- [3] S. Amstutz. The topological asymptotic for the Navier-Stokes equations. *ESAIM : Control, Optimisation and Calculus of Variations*, 11(3) :401–425, 3 2010.
- [4] S. Amstutz, I. Horchani, and M. Masmoudi. Crack detection by the topological gradient method. *Control and Cybernetics*, 34(1) :81–101, 2005.
- [5] G. Aubert and A. Drogoul. Topological gradient for a fourth order operator used in image analysis (To appear COCV).

- [6] G. Aubert and A. Drogoul. Topological gradient for fourth order pde and application to the detection of fine structures in 2d images. *C. R. Math. Acad. Sci. Paris*, 352 :609–613, 2014.
- [7] G. Aubert and P. Kornprobst. *Mathematical Problems in Image Processing : Partial Differential Equations and the Calculus of Variations (second edition)*, volume 147 of *Applied Mathematical Sciences*. Springer-Verlag, 2006.
- [8] Gilles Aubert and Jean-François Aujol. A variational approach to removing multiplicative noise. *SIAM Journal of Applied Mathematics*, 68(4) :925–946, 2008.
- [9] D. Auroux. From restoration by topological gradient to medical image segmentation via an asymptotic expansion. *Math. Comput. Model.*, 49(11-12) :2191–2205, 2009.
- [10] D. Auroux and M. Masmoudi. Image processing by topological asymptotic expansion. *Journal of Mathematical Imaging and Vision*, 33(2) :122–134, 2009.
- [11] D. Auroux, M. Masmoudi, and L. Jaafar Belaid. *Image restoration and classification by topological asymptotic expansion*, pages 23–42. *Variational Formulations in Mechanics : Theory and Applications*, E. Taroco, E.A. de Souza Neto and A.A. Novotny (Eds). CIMNE, Barcelona, Spain, 2007.
- [12] Didier Auroux and Mohamed Masmoudi. A one-shot inpainting algorithm based on the topological asymptotic analysis. *Computational & Applied Mathematics*, 25 :251 – 267, 2006.
- [13] H. Ayasso and A. Mohammad-Djafari. Joint image restoration and segmentation using Gauss-Markov-Potts prior models and variational Bayesian computation. In *16 th IEEE International Conference on Image Processing (ICIP)*, pages 1297–1300, 2009.
- [14] L. Jaafar Belaid, M. Jaoua, M. Masmoudi, and L. Siala. Image restoration and edge detection by topological asymptotic expansion. *C. R. Acad. Sci. Paris*, 342(5) :313 – 318, 2006.
- [15] L. Jaafar Belaid, M. Jaoua, M. Masmoudi, and L. Siala. Application of the topological gradient to image restoration and edge detection. *Engineering Analysis with Boundary Elements*, 32(11) :891 – 899, 2008.
- [16] S. Ben Hadj, L. Blanc Féraud, and G. Aubert. Space Variant Blind Image Restoration. *SIAM Journal on Imaging Sciences*, 7(4) :49, 2014.
- [17] S Bonettini, R Zanella, and L Zanni. A scaled gradient projection method for constrained image deblurring. *Inverse Problems*, 25(1) :015002, 2009.
- [18] T. Chan and J. Shen. *Image Processing And Analysis : Variational, Pde, Wavelet, and Stochastic*.
- [19] Nicolas Dey, Laure Blanc-Féraud, Christophe Zimmer, Pascal Roux, Zvi Kam, Jean-Christophe Olivo-Marin, and Josiane Zerubia. 3D Microscopy Deconvolution using Richardson-Lucy Algorithm with Total Variation Regularization. Rapport de recherche RR-5272, INRIA, 2004.
- [20] A. Drogoul. Numerical analysis of the topological gradient method for fourth order models and applications to the detection of fine structures in 2D imaging (To appear SIAM J. Imaging Sciences).
- [21] A. Drogoul. Topological gradient method applied to the detection of edges and fine structures in imaging. *Phd Thesis University of Nice Sophia Antipolis*, 2014.
- [22] Stuart Geman and Donald Geman. Stochastic Relaxation, Gibbs Distributions, and the Bayesian Restoration of Images. *IEEE Transactions on Pattern Analysis and Machine Intelligence*, 6(6) :721–741, 1984.
- [23] T. Hebert and R. Leahy. A generalized EM algorithm for 3D Bayesian reconstruction from Poisson data using Gibbs prior. *IEEE Trans. Medical imaging*, 8(2) :194–202, 1989.

- [24] Floyd M. Henderson, Anthony J. Lewis, and Robert A. Ryerson, editors. *Principles and applications of imaging radar*. Manual of remote sensing. Wiley, New York, 1998. Manual of remote sensing edited by Robert A. Ryerson.
- [25] M. Hintermüller. Fast-set based algorithms using shape and topological sensitivity information. *Control and Cybernetics*, 34(1) :305 – 324, 2005.
- [26] S.G. Johnson. Notes on fft-based differentiation. *MIT Applied Mathematics*, 2011.
- [27] Karl Krissian, Ron Kikinis, Carl-Fredrik Westin, and Kirby G. Vosburgh. Speckle-constrained filtering of ultrasound images. In *CVPR (2)*, pages 547–552. IEEE Computer Society, 2005.
- [28] S. Larnier and J. Fehrenbach. Edge detection and image restoration with anisotropic topological gradient. In *Proceedings ICASSP , International Conference on Acoustic Speech and Signal Processing*, pages 1362–1365, 2010.
- [29] S. Larnier, J. Fehrenbach, and M. Masmoudi. The topological gradient method : from optimal design to image processing. *Milan Journal of Mathematics*, 80(2) :411–441, 2012.
- [30] I. Larrabide, A.A. Novotny, R.A. Feijo, and E. Taroco. A medical image enhancement algorithms based on topological derivative and anisotropic diffusion. In *Proceedings of the XXVI Iberian Latin-American Congress on Computational methods in Engineering*, 2005.
- [31] S. Mallat. *A Wavelet Tour of Signal Processing*. Academic Press, 1998.
- [32] M. Masmoudi. The topological asymptotic. In *Computational Methods for Control Applications*, volume 16 of *GAKUTO Internat. Ser. Math. Appl., Tokyo, Japan*, 2001.
- [33] D. Mumford and J. Shah. Optimal approximations by piecewise smooth functions and associated variational problems. *Communications on Pure and Applied Mathematics*, 42(5) :577–685, 1989.
- [34] J. Pawley. *Handbook of Biological Confocal Microscopy*. Springer, Berlin, 2006.
- [35] Alex Sawatzky, Daniel Tenbrinck, Xiaoyi Jiang, and Martin Burger. A variational framework for region-based segmentation incorporating physical noise models. *Journal of Mathematical Imaging and Vision*, 47(3) :179–209, 2013.
- [36] J. Serra. *Image Analysis and Mathematical Morphology*. Academic Press, Inc., Orlando, FL, USA, 1983.
- [37] J. Sokolowski and A. Zochowski. On the topological derivative in shape optimization. *SIAM J. Control Optim.*, 37(4) :1251–1272, April 1999.
- [38] M Tur, K. C. Chin, and J. W. Goodman. When is speckle noise multiplicative ? *Applied Optics*, 21(7) :1157–1159, 1982.
- [39] M.N. Wernick and J.N.(eds) Aarsvold. *Emission tomography : The fundamental of PET and SPECT*. Elsevier, Amsterdam, 2004.